



**HAL**  
open science

## Evaluating the performance of multiple satellite-based precipitation products in the Congo River Basin using the SWAT model

V. dos Santos, R.A. Jucá Oliveira, P. Datok, S. Sauvage, A. Paris, M. Gosset, José Miguel SANCHEZ PEREZ

### ► To cite this version:

V. dos Santos, R.A. Jucá Oliveira, P. Datok, S. Sauvage, A. Paris, et al.. Evaluating the performance of multiple satellite-based precipitation products in the Congo River Basin using the SWAT model. *Journal of Hydrology: Regional Studies*, 2022, 42, pp.101168. 10.1016/j.ejrh.2022.101168 . hal-03826510

**HAL Id: hal-03826510**

**<https://hal.science/hal-03826510>**

Submitted on 26 Oct 2022

**HAL** is a multi-disciplinary open access archive for the deposit and dissemination of scientific research documents, whether they are published or not. The documents may come from teaching and research institutions in France or abroad, or from public or private research centers.

L'archive ouverte pluridisciplinaire **HAL**, est destinée au dépôt et à la diffusion de documents scientifiques de niveau recherche, publiés ou non, émanant des établissements d'enseignement et de recherche français ou étrangers, des laboratoires publics ou privés.

**Evaluating the performance of multiple satellite-based precipitation products in the** 1  
**Congo River Basin using the SWAT model** 2

V. Dos Santos<sup>a,\*</sup>, R. Oliveira<sup>b</sup>, P. Datok<sup>a</sup>, S. Sauvage<sup>a\*</sup>, A. Paris<sup>b,c</sup>, M. Gosset<sup>d</sup>, J. M. Sánchez- 4  
Pérez<sup>a</sup> 5

<sup>a</sup>Laboratoire Ecologie Fonctionnelle et Environnement, Institut national polytechnique de 6  
Toulouse (INPT), Centre National de la Recherche Scientifique (CNRS), Université de 7  
Toulouse (UPS). Avenue de l'Agrobiopole, 31326 Castanet Tolosan Cedex, France. 8

<sup>b</sup>Laboratoire d'Etudes en Géophysique et Océanographie Spatiales (LEGOS), UPS, CNRS, 9  
Centre National d'Etudes Spatiales (CNES), Institut de Recherche pour le Développement 10  
(IRD), 14 Avenue Édouard Belin, 31400 Toulouse, France. 11

<sup>c</sup>Hydro Matters, 1 Chemin de la Pousaraque, 31460 Le Faget, France 12

<sup>d</sup>Geoscience Environnement Toulouse (GET), IRD, UPS, CNRS, CNES, 14 Avenue Édouard 13  
Belin, 31400 Toulouse, France. 14

\* Corresponding authors 16

Email addresses: van.c.dossantos@gmail.com (V. Dos Santos), juca.oliveira@legos.obs- 17  
mip.fr (R. Oliveira) pankyesdatok@gmail.com (P. Datok), sabine.sauvage@univ-tlse3.fr (S. 18  
Sauvage), adrien.paris@hydro-matters.fr (A. Paris), marielle.gosset@ird.fr (M. Gosset), jose- 19  
miguel.sanchez-perez@univ-tlse3.fr (J. M. Sánchez-Pérez) 20

**Highlights:** 23

- Twenty-three satellite-based precipitation products were selected for this study from 24  
the Frequent Rainfall Observations on GridS (FROGS) daily precipitation database. 25

- We propose the use of a hydrological model to evaluate the performance of satellite-based precipitation products. 26  
27
- Precipitation over the Congo River Basin has large spatial and temporal variabilities that also have a significant contribution depending on the characteristics of the precipitation product under choice. 28  
29  
30
- Precipitation performances, in reproducing the annual cycle distributions, influence the model's abilities in simulating the water flow and water balance components. 31  
32
- The gauge-calibrated satellite performed better than satellite source for simulated streamflow taking the 3B42 v7.0 as reference. 33  
34

35

**Abstract:** Hydrological models have become practical tools to understand impacts in water resources and to support the development of management policies. Precipitation is a major driving force of hydrological processes and is one of the main input datasets for hydrological models. However, gauge measurements have several issues, such as incomplete areal coverage and deficiencies over most tropical regions. The precipitation data obtained by remote sensing is an alternative in areas where data is scarce or not available, like in the tropics. However, the feasibility of using satellite-based precipitation products for simulating streamflow needs to be verified, for different hydrological models and basins. Congo River Basin is one of the least studied major river basins in the world and suffers from the scarcity and difficulty in accessing rain gauge data, which makes satellite precipitation estimates necessary for hydrological studies. In this study, we analyzed twenty-three satellite-based precipitation products, acquired from Frequent Rainfall Observations on GridS (FROGS) daily precipitation database. We evaluated these precipitation products over the Congo River Basin using the hydrological model SWAT (Solid & Water Assessment Tool) for streamflow and water balance components at basin scale. Our findings showed that the products based on satellite-only source tend to

overestimate the rainy season peaks in comparison with the 3B42\_V7 product. On the other hand, the satellite products that consider gauge calibration presented better agreements between each other. The hydrological model was able to reproduce the general precipitation characteristics, while the gauge-adjusted satellite products performed better than those without gauge adjustments. Thus, the overall precipitation patterns have a crucial effect on model's performance and leads to different streamflow and water balance components values. The choice of rainfall product has a significant importance in the interpretation of the simulated hydrological cycle.

**Keywords:** precipitation, satellite observations, FROGS, SWAT model, Congo River Basin.

## 1. Introduction

Hydrological models are frequently used as practical tools to assess and to predict the impacts of anthropogenic activities on water resources and also assist in their management or create a basis for decision-making on sustainable development alternatives and conservation practices (Abbaspour et al., 2015, Loucks and Beek, 2017). However, these models require distributed meteorological information (precipitation, temperature, wind speed, etc.), which is a great challenge in large and poorly gauged areas such as tropical regions.

Precipitation is one of the main parameters for hydrological models, but its estimation is still very difficult, because of its strong spatio-temporal heterogeneity (Beck et al., 2016). There are three ways of measuring precipitation over a basin: (i) conventional instrumentation, using networks of rain (or snow) meters; (ii) ground based weather radar; and (iii) satellite measurement. Nevertheless, despite the accuracy of estimates from conventional instrumentation and weather radar, the distribution and density of these methods are highly variable. Another issue with these methods is the completeness and consistency of the historical

data series as well as the availability for near real-time analysis (Kidd and Levizzani, 2011, 76  
Sun et al., 2018). The precipitation data obtained by satellite is an alternative in regions where 77  
data is scarce, with a large number of free products available with high spatial and temporal 78  
resolution that can fill historical gaps and complement or replace in situ stations (Kidd et al., 79  
2017). With the advent of the satellite Tropical Rainfall Measuring Mission (TRMM, Huffman 80  
et al., 2007), from later 1997 to 2014, transitioning with the launch of the Global 81  
Precipitation Measurement (GPM, Hou et al., 2014; Skofronick-Jackson et al., 2017) Mission 82  
that is actually operating in conjunction with other passive microwave platforms, the 83  
performance of satellite precipitation estimates has significantly evolved along the years and 84  
numerous satellite-based precipitation products, with different characteristics (i.e., spatial, 85  
temporal, among others), have been developed and improved for distinct application purposes, 86  
such as for climatological, hydrological, agricultural and monitoring studies. Numerous 87  
observational daily precipitation products, including satellite estimates, are now available in a 88  
common  $1^{\circ} \times 1^{\circ}$  grid format through the Frequent Rainfall Observations on GridS (FROGS) 89  
database (Roca et al., 2019). FROGS database enables easier intercomparisons and 90  
applications, based on the selection of a single to multiple products considering their category 91  
(i.e., satellite-only, gauge-adjusted satellite estimates, among others). Nonetheless, the 92  
estimation of satellite precipitation data is not wholly reliable due to the uncertainties arising 93  
from measurement errors associated with observations, sampling, recovery algorithms and bias 94  
correction processes that leads to systematic and random errors (Roca et al., 2010, Oliveira et 95  
al., 2016, Beck et al., 2016, Beck et al., 2017, Sun et al., 2017). 96

Tropical forests, including the Congo River Basin (CRB), strongly influence both the regional 97  
and global climate, storing large carbon stocks and regulating energy and water cycles. In this 98  
sense, any changes in the structure of these ecosystems, such as those caused by deforestation, 99  
can create positive feedbacks and increase climate change trends (Kruijt et al. 2016). The CRB 100

in central Africa is the second-largest river basin in the world and supports one of Earth's three 101  
major humid tropical forest regions (Alsdorf et al., 2016); it contains about 70 percent of 102  
Africa's forest cover: Of the Congo Basin's 530 million hectares of land, 300 million are 103  
covered by forest. Almost 99 % of the forested area is primary or naturally regenerated forest 104  
as opposed to plantations, and 46 % is lowland dense forest. The average annual precipitation 105  
is around 1500 - 2000 mm of precipitation per year and is the most convectively active region 106  
of the world (Dezfuli, 2017). Almost 60% of precipitation occurs during the wet seasons and 107  
the basin-wide average seasonal cycle has two precipitation peaks, one in March and the other 108  
in November (Hua et al. 2019, Crowhurst et al., 2020). This basin is currently an object of 109  
concern because of evidence of a significant multidecadal drying trend, one of the most 110  
significant worldwide (Zhou et al., 2014, Harris et al., 2017). Despite the important role in the 111  
tropical climate system, the CRB is plagued by a scarcity of precipitation ground-data 112  
especially after the early 1990s. Since the meteorological services of both Angola and the 113  
Democratic Republic of the Congo; countries that include most of the Congo rain forest, 114  
essentially ceased to function for decades and have been slow to rebuild their services (Alsdorf 115  
et al., 2016). The lack of in situ data leads most hydrological studies in the Congo basin to 116  
depend on satellite precipitation estimates. 117

It is essential to verify the quality and the applicability of precipitation data derived from multi- 118  
satellites through statistical evaluation strategies. The variability of precipitation plays a key 119  
role in determining the hydrological response of river basins. We assume that the river 120  
streamflow follows the variability of rainfall and we propose to use a hydrological model to 121  
evaluate the performance of multiple and distinct precipitation products. This study aims to 122  
contribute to the debate on the performance of satellite precipitation estimates that are based 123  
on different techniques. To achieve that, specifically this study aims to (i) analyze and 124  
intercompare the precipitation distribution characteristics from 23 satellite-based precipitation 125

products over the CRB during the period from 2001 to 2012 from FROGS database; (ii) 126  
evaluate the selected satellite precipitation products' skills in simulating the streamflow and 127  
water balance components through a hydrological model, SWAT (Soil & Water Assessment 128  
Tool, Arnold et al. 1998) at monthly time scale. Thus, this article is organized as follows. In 129  
Section 2 we describe the study area, the precipitation database and the methodology. Section 130  
3 provides an assessment and discussion of the selected precipitation products, which are 131  
subsequently applied through the SWAT model, and which are exploited in the same section. 132  
Finally, the conclusions are presented in Section 4. 133

## 2. Materials and Methods 134

### 2.1. Study Area and data 135

The intracratonic depression in Central Africa called the CRB (Figure 1) is situated between 136  
latitudes 9°N and 14°S and longitudes 11°E and 34°E. It covers an area of approximately 3.7 137  
million km<sup>2</sup> including most of the Democratic Republic of Congo, (DRC, formerly Zaire), the 138  
People's Republic of Congo (ROC) and the Central African Republic (CAR). Elevations within 139  
the basin are above 3000 meters above sea level (m asl) in the Eastern highlands and less than 140  
300 m asl in the center of the basin (Runge et al., 2007). The physiography of the CRB varies 141  
and consists of the northern peneplains of bushy/wooded savanna with tropical humid climate 142  
(Bultot, 1971). The middle basin includes the dense and heavily forested swamp forest of the 143  
Cuvette Centrale, and the sandy sandstone formations of the Batékés Plateaux of between 350 144  
– 930 meters altitude covered by bushy savanna (Laraque et al., 2001). 145

### Figure 1. 146

Mean annual rainfall is 2000 mm/y<sup>-1</sup> in the central basin decreasing northward to southward to 150  
1100 mm/y<sup>-1</sup> (Alsdorf et al., 2016). The basic rainfall pattern across the basin is thought to be 151  
due to the bi-annual passage of the inter-tropical convergence zone (ITCZ) across the basin. 152  
The ITCZ over Africa is acknowledged as the location where the dry northeasterly harmattan 153  
meets the moist southerly flow of the monsoon and a major control on tropical rainfall. Recent 154  
evidence concerning the latitudinal progression of the equatorial rainy season however suggests 155  
that this view of the ITCZ may be challenged (Jackson et al., 2009; Nicholson et al., 2019). 156  
Rainfall across the basin occurs with a seasonal peak in Precipitation from December to March 157  
in areas of the southern hemisphere with northern hemisphere basins having theirs within July 158  
to October (Moukandi et al., 2021). Annual extremes of precipitation in the equatorial regions 159  
are in April and October while sharp precipitation gradients, which may result in spurious 160  
trends, are noticed in the south-Eastern parts of the basin (Yin and G, 2010; Tshimanga et al., 161  
2012). 162

## 2.2. Satellite-Based Precipitation Datasets 163

Twenty-three precipitation products, with a common period from 2001 to 2012 (except 3B42 165  
v7.0, period from 1998 to 2012), were selected for this study (Table 1). These datasets were 166  
acquired from The Frequent Rainfall Observations on GridS (FROGS) database (Roca et al., 167  
2019). FROGS is composed of several quasi-global and regional daily precipitation products 168  
with a common spatial resolution of 1° × 1°. Although FROGS database includes satellites, 169  
ground-based and reanalysis products, only the satellite-based category was considered for this 170  
study. The satellite-based precipitation products, which differ from each other in multiple 171  
aspects (e.g., satellite source, with or without gauge adjustments, among others), are here sub- 172  
divided into two main groups: i) the satellite-only and ii) the gauge-calibrated satellite. These 173  
products are retrieved utilizing infrared (IR) observations from geostationary satellites and/or 174



passive microwave observations from multiple or single low elevation orbiting (LEO) 175  
satellites. The gauge-based calibration step is distinctly applied to those satellite precipitation 176  
products. These adjustments are climatological on a monthly or daily time step and take into 177  
consideration in-situ observations from the Global Telecommunication System (GTS) or other 178  
gauge-based precipitation products (e.g., GPCC). Table 1 shows the satellite-based 179  
precipitation products selected for this study and their main characteristics. FROGS database 180  
is freely available from <ftp://ftp.climserv.ipsl.polytechnique.fr/FROGS/>. See Roca et al. (2019) 181  
for a detailed description of each product. 182

**Table 1.** 184

### 2.3. SWAT Model 187

The soil & Water Assessment Tool is a continuous-time, spatially distributed hydrological 188  
basin scale model that simulates water, sediment, nutrient, chemical, and bacterial transport in 189  
a basin resulting from the interactions among weather condition, soil properties, stream channel 190  
characteristics, vegetation and crop growth, as well as land-management practices. The model 191  
calculates pollutant loads from various non-point and point sources (Arnold et al., 1998). 192  
Fundamentally, the model is hydrologically driven, based upon the water balance of an 193  
individual landscape unit: 194

$$SW_t = SW_0 + \sum_{i=1}^t (R_{dayi} - Q_{surfi} - E_{ai} - w_{seepi} - Q_{gwi}) \quad (1) \quad 196$$

where  $SW_t$  is the final soil water content (mm H<sub>2</sub>O);  $SW_0$  is the initial soil water content (mm 198  
H<sub>2</sub>O);  $t$  is time (days);  $R_{dayi}$  is precipitation on day  $i$  (mm H<sub>2</sub>O);  $Q_{surfi}$  is surface runoff on day 199

$i$  (mm H<sub>2</sub>O);  $E_{ai}$  is evapotranspiration on day  $i$  (mm H<sub>2</sub>O);  $w_{seepi}$  is the amount of water from the soil profile inflowing to the vadose zone on day  $i$  (mm H<sub>2</sub>O); and  $Q_{gwi}$  is the base flow on day  $i$  (mm H<sub>2</sub>O).

### 2.3.1. Model Setup

SWAT2012 version (Winchell et al., 2013) was set up for the CRB using the datasets listed in Table 2. The basin was delineated based on the dominant land use, soil and slope classes taking into cognizance the size and spatial heterogeneity of the basin allocating one Hydrologic Response Unit (HRU) per subbasin resulting in 272 subbasins and HRUs. The period of simulation was from 1998 to 2012, comprising calibration (2000-2006), validation (2006-2012), and a two-year warm-up period (1998-2000).

In the SWAT model, the evapotranspiration is calculated using the Penman-Monteith method. The Penman-Monteith method also gave better estimates of evapotranspiration when used with the plant growth modification of Strauch and Volk (2013). The plant growth module was used since the SWAT model simulates plant growth based on dormancy during the winter season for the reinitiation of the growing season for perennial plants and this process is not a valid growing pattern in the tropics. The surface runoff was calculated using the Soil Conservation Service's Curve Number method (USDA Soil Conservation Service, 1972) and the variable storage method (Williams, 1969) was used for channel routing.

### Table 2.

### 2.3.2 Model calibration

Model calibration was based on the optimization of the parameter values by adjusting the simulated streamflow ( $Q_{sim}$ ) at observed streamflow ( $Q_{obs}$ ). The monthly  $Q_{obs}$  data from the

five gauging stations (Figure 1) were available for the period 2000-2012 (Table 2). In the model set-up used in this study, the simulated streamflow was adjusted to the observed streamflow by manual calibration (trial and error). Further details of the calibration and validation procedures can be found in Datok et al. (2021).

For the evaluation of model performance, we used the Nash and Sutcliffe (1970) efficiency (NSE) that measures the magnitude of residual variance, compared to observed variance (Moriasi et al., 2007); the coefficient of determination ( $R^2$ ) that describes the degree of linear relationship between observed and simulated streamflow and percent bias (PBIAS) which evaluates the average tendency of the magnitude of simulated values in relation to the observed ones. Kling–Gupta efficiency (KGE) by Gupta et al., (2009), which provides decomposition of NSE and mean squared error; KGE facilitates the analysis of relative importance of correlation, bias, and variability in hydrologic modeling (KGE-hydroGOF, 2017). For streamflow, Moriasi et al. (2015) proposed NSE values  $> 0.50$ ,  $R^2 > 0.60$  and  $PBIAS < \pm 25$  to be a satisfactory level for monthly scales. A KGE value  $> 0.50$  is also considered satisfactory (Gupta et al., 2009).

#### 2.4. Evaluation of the performance of precipitation datasets using SWAT model

The SWAT model was run for twenty-three scenarios based on the precipitation products described in Table 1. The base scenario is based on the 3B42\_v7.0 product and it was calibrated with observed streamflow (see above). The others precipitation scenarios were run using identical datasets (see Table 1) so that variations in streamflow and other hydrological components were uniquely attributable to precipitation. For the evaluation of the performance of precipitation datasets, we used KGE and PBIAS objective functions calculated using the streamflow of base scenario (3B42\_v7.0) as reference.

### 3. Results and Discussion 250

Precipitation regimes over the CRB are firstly assessed through the 23 satellite-based 251  
precipitation products during the period from 2001 to 2012. Secondly, the model calibration 252  
and validation are performed for the period from 1998 to 2012 (two-years of warm-up for the 253  
model). Afterwards, hydrological evolution (streamflow and water balance components) 254  
through the 23 precipitation products during 2003 to 2012 (two-years of warn-up) are assessed. 255  
Finally, we discuss the influence of the precipitation input on model performance when the 256  
model has been pre-calibrated with one of the products (here 3B42). 257

#### 3.1. Comparison of the different precipitation datasets 259

Satellite precipitation estimates, through different gridded products, has been constantly 260  
evaluated and assessed across West Africa, considering gauged-precipitation observations as a 261  
reference (e.g., Gosset et al., 2018, Nicholson et al., 2019, Satgé et al., 2020). The reliability 262  
of satellite precipitation estimates depends on several factors (e.g., seasonality, the gauge 263  
network densities) and can vary in space and time. The precipitation regime (i.e., seasonality) 264  
over the CRB varies regionally (e.g., Munzimi et al., 2015). Spatially, there are remarkable 265  
characteristics on the precipitation distribution over CRB, which are demonstrated through the 266  
unconditional annual mean and the 99th percentile (Figure 2). The central region of the CRB 267  
and the northern portion of the Luabala sub-basin experience the largest amounts of 268  
precipitation with about 7 and 10 mm day<sup>-1</sup>, respectively. Nevertheless, the Luabala also 269  
showed the largest regional contrast of precipitation amounts, with most of the watershed area 270  
presenting precipitation mean lower than 3 mm day<sup>-1</sup>. These spatial characteristics were 271  
directly linked to the extreme precipitation occurrences, represented by the 99th percentile, 272  
strongly influenced by the surface type (i.e., orographic) conditions, where the highest values 273  
(>50 mm day<sup>-1</sup>) were found mainly across the wetland zones and over the northwest part of 274

Luabala. Figure 3 depicts the annual cycle of precipitation, through the monthly accumulated 275  
mean distributions, from all the selected satellite-based precipitation products over the five 276  
CRB sub-basins, during the period from 2001 to 2012. The contrasts between the satellite-only 277  
and satellite gauged-adjusted precipitation are assessed considering the 3B42\_v7.0 product as 278  
baseline. Overall, three different precipitation regimes, which were associated with the 279  
geographic characteristics, were observed across the five Congo's sub-basins, which is in 280  
agreement with previous findings based on both the satellite and rain gauge data (e.g., Munzimi 281  
et al., 2015): i) Kasai and Luabala, located in the southernmost portion, presenting a well- 282  
defined dry/wet period, with the maximum (minimum) from November to March (between 283  
June and August); ii) Sangha and Ubangi, in the northern portions, present a prolonged rainy 284  
period (peak of maximums around August/September) and a short-term dry season (December 285  
and January); and iii) the central part, which is characterized by a less well-defined monsoonal 286  
regime, with a dry period less pronounced and two rainy peaks (the first around March and the 287  
second during October/November). 288

Although all the satellite precipitation products were able to successfully represent the annual 289  
cycle of rainfall over each watershed under study, notable differences along the year on the 290  
magnitudes of the precipitation amounts were observed. Overall, two remarkable performance 291  
characteristics were noted. The group of satellite-only products mostly overestimates the rainy 292  
seasons' peaks compared to the rest of the products. In particular, the CMORPH\_v1.0\_RAW, 293  
3B42RT\_UNCAL\_v7.0, followed by IMERG\_V06\_EU and IMERG\_V06\_LU products stand 294  
out for presenting the highest peaks, especially during the rainy seasons, systematically for all 295  
the five sub-basins. For instance, CMORPH\_v1.0\_RAW overestimates about 100 mm/month, 296  
in comparison to the rest of the products, at most of the sub-basins. On the other hand, the 297  
group of gauge-adjusted satellite products presented better agreements between each other and 298  
compared to 3B42\_v7.0, except for GSMAP-gauges-RNLv6.0 and CMORPH\_v1.0\_CRT, 299

which exhibited opposite performances to its satellite-only versions, underestimating the 300  
monthly totals during a greater part of the year for all the five sub-basins. In addition, 301  
TAMSAT\_v2 stands out due to its difficulties in following the annual cycle properly (e.g., 302  
Central), underestimating the rainiest months at all sub-basins and also overestimating drier 303  
periods, especially over the northern portions (i.e., at Sangha and Ubangi). 304

**Figure 2.** 305

**Figure 3.** 306

Other particular basin characteristics and the performance diversities of both the satellite-only 310  
and gauge-adjusted products are clear considering the relative differences (%) of each product 311  
compared to 3B42\_v7.0 as reference (in Supplementary Material, Figure S1). The 312  
overestimations found by satellite-only products were relatively larger during the dry and dry- 313  
to-wet periods over Kasai and Luabala sub-basins. In this case, during these periods at Luabala, 314  
the 3B42\_IR\_v7.0, 3B42RT\_UNCAL\_v7.0 and CMORPH\_v1.0\_RAW products stand out for 315  
presenting the largest relative differences among all the sub-basins, with more than 300 %, 316  
200 % and about 290 %, respectively. An opposite behavior, with negative relative differences 317  
(in about -100%) during the dry period at Kasai and Luabala sub-basins, was observed for the 318  
gauge-adjusted satellite group, with slight exception 3B42RT\_v7.0 and CMORPH\_v1.0\_CRT 319  
(at Luabala). The regional TAMSAT\_v2.0, TAMSAT\_v3.0 and ARC2 products, in 320  
comparison to 3B42\_v7.0 product, tend to overestimate January's amounts of precipitation (the 321  
dry period) at Sangha and Ubangi, which are consistent with the findings of Ayehu et al., (2018) 322  
for another African region. 323

It is worth mentioning that the performance and/or agreement of certain satellite precipitation 324  
products, in particular the native versions (satellite-only) and those ones adjusted/calibrated by 325  
rain gauges, in representing the local and/or regional precipitation regimes, are extremely 326  
linked to the region of interest. This is because the precipitation regimes are driven by multiple 327  
factors, including the frequency and intensity of rainy/non-rainy days to its monthly totals, as 328  
well as the contribution of a certain class of precipitation occurrences and the corroboration of 329  
moderate-extreme and extreme events over tropical land regions (Roca, 2019). These factors 330  
can be represented differently by satellite estimates and the differences are related to distinct 331  
aspects (e.g., the product technique itself, platform sources, gauge-adjustments, systematic 332  
uncertainties, among others). 333

Figure 4 shows the cumulative density functions (CDF) of occurrence and volume (amount) of 334  
daily precipitation during the period from 2001 to 2012 over the five Congo sub-basins 335  
computed for each satellite precipitation product (satellite-only and satellite gauge-adjusted) 336  
acquired from FROGs database. Through the overall CDF analyses, it becomes more evident, 337  
the differences between the two groups of satellite precipitation compared to the 3B42\_v7.0 338  
reference database. It is also possible to note that, even though the monthly totals are impacted 339  
differently, these two distinct CDF distributions are preserved for all the five watersheds. Better 340  
agreements between all the satellite-only products compared to the 3B42\_v7.0, in both the 341  
occurrences and amounts of precipitation distributions, were observed. Slight overestimations 342  
(underestimations) on the amounts (occurrences) frequencies of rainfalls lower (greater) than 343  
 $\sim 5 \text{ mm day}^{-1}$  were observed from most of the satellite-only products compared to 3B42\_v7.0. 344  
However, the ARC2 and CHIRP\_V2 products presented opposite features, especially at the 345  
Luabala and the Central basins respectively. In contrast, the group of gauge-adjusted satellite 346  
precipitation products showed larger differences (heterogeneities) across all precipitation 347  
distribution ranges, especially in the volume of precipitation frequencies (e.g., up to 45 % of 348

frequency differences at precipitation intensities from 1 to 5 mm day<sup>-1</sup>). In parallel to the scattered frequency distributions on the rainfall occurrences, an overestimation, most prominent at rainfall intensities greater than 10 mm day<sup>-1</sup>, were observed from almost all the satellite+gauge products in comparison to 3B42\_v7.0, except for CMORPH\_v1.0\_CRT (at Luabala) and TAMSAT\_v2 (at Sangha and Ubangi). Such characteristics suggest that the gauge inclusion and/or adjustment techniques could directly impact quantitatively and qualitatively the daily precipitation distributions, from low to larger intensities, modifying its amount and occurrence frequencies.

#### Figure 4.

### 3.2. Model Calibration and Efficiency

The statistical results and graphical comparisons of the simulated SWAT calibration and validation aggregated monthly streamflow ( $Q_{sim}$ ) versus corresponding measured streamflow ( $Q_{obs}$ ) are listed in table 3 and shown in figure 5 for all gauge sites (Figure 1). The NSE,  $R^2$  and KGE values for the calibration and validation periods for Ubangi/Bangui and Sangha/Ouessou gauges suggest good model performance. For Kasai/Kutu-Moke and Brazzaville/Kinshasa (outlet) gauges, these values suggest acceptable model performance, but for Lualaba/Kisangani the model, performance is less acceptable. The Ubangui and Sangha basins, mostly draining the northern hemisphere, present few hydrological and hydraulic singularities, thus it is not surprising that the conversion of rainfall into discharge is well performed by the model. The Lualaba sub-basin presents many lakes and swamps, including the Tanganyika lake which behavior was complicated to model due to the lack hydraulic / hydrological data (e.g. volume of water stored, surface area) for these lakes. PBIAS suggest good fit between simulated and observed streamflow for all gauge sites. However, the PBIAS indicated an underestimation for



the calibration period, except for Kasai/Kutu-Moke gauge; and overestimation for the 374  
validation period, with the exception of the Brazzaville/Kinshasa (outlet) gauge. 375

**Table 3.** 377

Figure 6 shows the relative error between  $Q_{obs}$  and  $Q_{sim}$  (positive values indicate overestimated 379  
 $Q_{sim}$  and negative values indicate underestimated  $Q_{sim}$ ). For Ubangi/Bangui, Sangha/Ouesso, 380  
and Kasai/Kutu-Moke, the model in general overestimated low flows in  $Q_{obs}$  in the calibration 381  
and validation periods. Conversely, for Lualaba/Kisangani and Brazzaville/Kinshasa (outlet) 382  
the model underestimated low flows periods. The peak flow at Brazzaville/Kinshasa (outlet) 383  
was underestimated, while for other gauges the peak flow was slightly underestimated. The 384  
overestimation of minimum values of  $Q_{obs}$  is linked to the lower baseflow and faster recession 385  
during the dry season. This overestimation could not be corrected by an increase of baseflow 386  
recession constant, because it would lead to overestimating streamflow during the beginning 387  
of the rainy season. Further details about the drainage sub-basins and calibration and validation 388  
can be found in Datok et al. (2021). 389

**Figure 5.** 391

**Figure 6.** 393

3.3. Hydrological evaluation 395

3.3.1. *Streamflow* 396

The hydrographs (Figure 7) indicate that the SWAT model follows the key features of the 397  
satellite precipitation products as the dry and wet season at the five-gauge sites studied, and 398

thus, it is possible to evaluate the performance of those products without recalibration. It is 399  
expected however that the twenty-two precipitation products inputs lead to different 400  
streamflow prediction than the 3B42\_v7.0 (base scenario) at all five-gauges. In general, and as 401  
expected, the products without precipitation adjustments (satellite-only) predicts higher 402  
streamflow. However, according to the results some satellite products behave differently, for 403  
example CMORPH\_v1.0\_CRT predicts higher streamflow at the gauge Lualaba/Kisangani, 404  
but in other gauges, this product underestimated the streamflow. 405

Statistical analysis (Figure 8) and the  $\Delta\%$  (Supplementary Material—Table S2) demonstrated 406  
that the hydrological model driven by the precipitation products with precipitation adjustments 407  
(satellite+gauge) performed better than those without precipitation adjustments; as expected, 408  
but trends between the products and differences between the regions are evident. The KGE and 409  
PBIAS indexes indicates some products can provide satisfactory performance at 410  
Ubangi/Bangui, Lualaba/Kisangani and Brazzaville/Kinshasa (outlet) without model 411  
recalibration. Figure 8 also highlights that GPCP\_CDR\_v1.3\_not\_enforced, which it is a 412  
satellite only product, demonstrates a good performance (KGE 0.71) at Ubangi/Bangui gauge. 413

When looking at the entire CRB, the worst scores were obtained by 3B42RT\_UNCAL\_v7.0 414  
and CMORPH\_v1.0\_RAW satellite-only products. It is evidenced by Figure 8 that while some 415  
satellite-only products tend to lead to higher streamflow predictions (such as 416  
CMORPH\_v1.0\_RAW and 3B42RT\_UNCAL\_v7.0), others as 3B42\_IR\_v7.0 and 417  
3B42\_MW\_v7.0 tend to lead to lower streamflows in particularly at Sangha/Ouessou and 418  
Ubangi/Bangui dry regions of CRB. The regional products (TAMSAT v2.0, v3.0 and ARC2) 419  
did not perform well in estimating streamflow, when compared to quasi-global products such 420  
as the IMERG\_v6.0\_FC or land-only products like the CHIRPS\_v2.0. Although ARC2 421  
performed better than the other regional products, it still did consequently underestimate the 422  
streamflow at four-gauge stations. 423

The near-real-time (NRT) precipitation products (important for now-casting and forecasting streamflow in applications such as early warning systems) such as IMERG\_v6.0\_EU and IMERG\_v6.0\_LU did not provide a good prediction of streamflow, showing a consequent overestimation at all gauges. Among the NRT products, only 3B42RT\_v7.0 had a good performance at the Ubangi/Bangui stations, and Brazzaville/Kinshasa (outlet) and Kasai/Kutu-Moke. The PBIAS indicates a good performance when compared to the base scenario, maybe due to the similarities with the product used in our base scenario.

In general, the monthly streamflow simulation results and the statistical scores from IMERG\_v6.0\_FC and CHIRPS\_v2.0 presented consistent streamflow simulations, except for Kasai/Kutu-Moke and Sangha/Ouessou gauges. Studies as Tan et al. (2018) and Amorim et al. (2020) have shown the better performance of IMERG products to estimate streamflow all around the world in comparison to TMPA products, due to its improvement in precipitation estimation. In our case, the recalibration of model parameters for IMERG products could improve streamflow simulations, specifically at the gauge stations where 3B42\_v7.0 did not perform well.

**Figure 7.**

**Figure 8.**

### *3.3.2. Water balance components*

To better understand the influence of the different precipitation products in predicting the water balance components (WBC) utilizing the SWAT model, we analyzed the monthly cycle of evapotranspiration (ET), surface runoff (SURQ), lateral flow (LATQ), percolation (PERC), soil water content (SW), groundwater contribution to streamflow (GWQ) and water yield

(WYLD) simulated at the sub-basin scale. The results show that the satellite-only products tend 449  
to overestimate the WBC, especially in the rainy season. However, the level of overestimation 450  
and underestimation depends on the type of WBC and the region in the CRB. 451  
For ET predictions (Figure 9), the precipitation products have the tendency to overestimate in 452  
both dry and wet seasons when compared to 3B42\_v7.0, although some track ET much more 453  
closely than others. The CMORPH\_v1.0\_RAW and GSMAP\_gauges\_RNL\_v6.0 have the 454  
tendency to underestimate this component. Peak basin-wide ET during March is 455  
overestimated for almost all products, while the basin's low at June, July and August is 456  
underestimated at Lualaba and overestimated at other regions. At Ubangi, most of the 457  
precipitation products capture the same tendency of 3B42\_v7.0 between June to February. 458  
Overall, the global ET prediction is overestimated at all sub-basins (in Supplementary Material, 459  
Table S3). 460

### Figure 9.

The SURQ (Figure 10), LATQ and PERC (Supplementary Material - Figures S4 and S5) 464  
predictions, -which are intrinsically linked to the amount and dynamics of precipitation- are 465  
similar for the dry season at Kasai, Ubangi and Sangha sub-basins. However, none of the 466  
products capture the full amplitude of fluctuations across seasons at the Central and Lualaba 467  
sub-basins. The predictions are overestimated even in the dry season. For the wet season, the 468  
satellite precipitation products have the tendency to overestimate these components in regards 469  
to 3B42\_v7.0 at five regions. Kasai and Lualaba sub-basins presenting one large peak of 470  
SURQ, LAT and PERC between November to March. Sangha and Ubangi have one peak 471  
around August/September while the Central region has two peaks, the first around March/April 472  
and the second during October/November. These peaks are overestimated and some products 473

as TAMSAT\_v3.0 and ARC2 do not follow the same seasonal shape of 3B42\_v7.0. In general, 474  
the global SURQ, LATQ and PERC (in Supplementary Material, Table S3) are overestimated, 475  
although some track much more closely than others, especially in the dry season. 476

**Figure 10.** 478

The SW (Figure 11) and GWQ (Supplementary Material - Figure S6) predictions, - which 480  
refers to water stored in soil - demonstrate a wide range of simulated values, particularly for 481  
GWQ, hence overestimates of these components for both satellite-only and satellite+gauge 482  
with respect to 3B42\_v7.0. SW the precipitation products generally follow the seasonal shape, 483  
except some products as CMORPH\_v1.0\_RAW and GSMAP\_gauges\_RNL\_v6.0 although 484  
none of them capture the full amplitude of fluctuations across seasons. The tracks are closer 485  
than others for SW in the dry season at Lualaba and Ubangi, but for Central, Kasai and Sangha, 486  
the tracks are scattered. 487

**Figure 11.** 489

The seasonal cycle of GWQ does not present a large fluctuation across seasons, but the tracks 491  
are scattered at all regions studied. This behaviour could be linked to the SWAT model, because 492  
the model simulates groundwater using the two-way groundwater-surface water exchange 493  
which limits the ability to predict groundwater storage (Malaku and Wang, 2019, Shao et al., 494  
2019). Also, the surface water-groundwater interaction mechanisms are less studied than other 495  
WBC in the Congo Basin (Alsdorf et al., 2016). 496

The WYLD (Supplementary Material—Figures – S6) predictions (consisting of: surface runoff 497  
+ groundwater flow + tile flow – transmission loss) are also overestimated compared to 498

3B42\_v7.0. The peak flows have the same characteristic of SURQ at all regions, with two 499  
peaks at the Central, Kasai and Lualaba. However, peak shapes of some precipitation products 500  
are wider than the peak of 3B42\_v7.0. Similar to the GWQ, the WYLD tracks are scattered at 501  
all sub-basins. 502

Overall, the trends between the precipitation products and differences between the regions 503  
affects the WBC. The  $\Delta\%$  (Supplementary Material—Table S3) showed that even a small 504  
increase or decrease of amounts of precipitation would cause increase or decrease in the WBC, 505  
especially the components that are dependent on the dynamics of precipitation as surface runoff 506  
and percolation. However, some precipitation products behave differently, for example, in most 507  
of the analyzed products, an increase in amount of precipitation leads to an increase in the 508  
values of the WBC, but CMORPH\_v1.0\_CRT shows a decrease of amount of precipitation 509  
then an increase in surface runoff values at the Central, Kasai and Sangha, that leads to a 510  
decrease of percolation. Several possible causes could lead to these results, the hydrological 511  
response of the WBC is linked to precipitation and design and assumptions of the model to 512  
type of vegetation, topography and soil. It is expected that in forest areas there will be less 513  
surface runoff than in pasture areas for example. Soil degradation will also lead to an increase 514  
of runoff. 515

### 3.4 Influence of the precipitation input on model performance 516

The SWAT model was originally based on the climate and environmental conditions in the 518  
United States, and it proved to be an effective tool to evaluate land management practices in 519  
floodplains and agricultural chemicals and water resources over other regions around the world 520  
(e.g.: Wei et al., 2019, Cakir et al., 2020, Sok et al., 2020). However, SWAT requires certain 521  
improvements before it can be applied in tropical regions; such as improvements to crop and 522  
soil parameters. Nonetheless, several studies in tropical regions reported good performance of 523

this model, especially at monthly time step (e.g.: Dos Santos et al., 2018, Galavi and Mirzaei, 2020, Tan and Yang 2020, Mandal et al., 2021).

To compare the hydrological performance of the satellite-based precipitation products using the SWAT model, we summarized some recent hydrological evaluation studies around the world in Table 4 (Tuo et al., 2016, Tan et al., 2018, Amorim et al., 2020, Sharannya et al., 2020, Peng et al., 2021, Wang et al., 2021). Four main conclusions can be drawn from the comparisons: i) in many cases, the IMERG\_v6.0\_FC outperforms 3B42\_v7.0 in hydrological simulations due to its improvement in precipitation estimation; ii) the performance of the satellite-based precipitation products depends on the basin localization and simulations scale (daily or monthly); iii) hydrological model choice will affect the accuracy assessment of precipitation products for detecting streamflow extremes; and iv) the recalibration of the model parameters for each satellite-based precipitation product effectively improved the precision of streamflow simulations.

#### **Table 4**

As shown in the hydrological evaluation section, the IMERG\_v6.0\_FC and CHIRPS v2.0 products demonstrates good performance without recalibration and could be used to study the hydrological cycle in the CRB, especially for streamflow and evapotranspiration. These results agree with the findings reported in Table 4, and a recalibration of the model parameters could effectively improve the precision of satellite-based precipitation product simulations, especially for WBC that are connected to the amount and dynamics of precipitation as SURQ, LATQ and PERC.

Nevertheless, the bias in satellite-based precipitation products was recognized as a major issue across several basins around the world (Maggioni and Massari, 2018), and the inaccuracy of

satellite data may lead to unrealistic parameter values when recalibrating the model (Peng et al., 2021). Maggioni and Massari (2018) have shown that model recalibration was also raised as a viable option to improve streamflow simulations from satellite-based precipitation products, but caution is necessary when recalibrating models. Another option is the bias correction of the satellite products with ground-based measurements of precipitation to obtain more realistic flow simulations (Wang et al., 2021). However, satellites estimate appear to not perform well over the CRB (McCollum et al., 2000; Awange et al., 2016) and there are large discrepancies between gauge-based products from GPCP (Global Precipitation Climatology Project), and CPC (Climate Prediction Center) in the interannual and decadal variations in precipitation over the basin (Negron Juarez et al., 2009). The lack of a dense and reliable network of rain gauges makes it impossible to assess quantitatively the rainfall products against a proper ground validation reference. In addition, for the long-term mean, GPCP and CMAP display the major precipitation patterns, although substantial discrepancies occur in areas with low gauge densities, such as equatorial West Africa (Yin et al., 2004). However, independent of these discrepancies, our findings show that the IMERG\_v6.0\_FC and CHIRPS v2.0 are potential alternative sources of data for hydrological modeling using SWAT in the CRB.

#### **Table 4.**

#### **4. Conclusions**

The present work investigated the performances of 23 satellite-based precipitation products (Table 1) in simulating streamflow and water balance components at the Congo River Basin through the SWAT model. The key findings are as follows:



The precipitation products were able to represent with consistency the annual cycle of rainfall 574  
and the frequencies of rain intensities/occurrences over each sub-basin studied. However, the 575  
precipitation amount magnitudes along the year are different, especially due to high 576  
precipitation intensities. In the absence of a reliable dense ground validation network, the gauge 577  
adjusted version of 3B42\_v7.0, which has been shown to provide good simulations of the 578  
discharge through the SWAT model, was taken as a benchmark to analyze the skills of other 579  
precipitation products. Overall, the group of satellite-only precipitation products mostly 580  
overestimates the rainy season peaks; and the gauge-adjusted satellite products presented better 581  
agreements between each other and compared to 3B42\_v7.0, except for GSMAP-gauges- 582  
RNLv6.0 and CMORPH\_v1.0\_CRT. 583

Streamflow and water balance components simulation replicate precipitation products patterns, 584  
and gauge-adjusted satellite performed better than satellite-only for streamflow. In addition, 585  
during the rainy season, the precipitation products have the tendency to overestimate the 586  
SURQ, LATQ and PERC in regards to 3B42\_v7.0 over the Congo Basin. For others 587  
components (ET, SW, GWQ and WYLD) and streamflow predictions, there is an 588  
overestimation at all sub-basins. However, IMERG\_v6.0\_FC and CHIRPS v2.0 products 589  
demonstrate good performance with our model, and could be used to predict the hydrological 590  
cycle. 591

In general, the selection of precipitation products has a crucial effect on model performance 592  
and has to be taken into consideration since it is one of the sources of uncertainties. 593  
Unfortunately, the Congo River Basin is deprived of a quality and dense rain gauge network 594  
for assessing these uncertainties more quantitatively. Using the hydrological model with an 595  
ensemble of available products provides a good illustration of the impact of the uncertainties 596  
and can be used to filter out the products which behave like outliers and/or to indicate the 597  
confidence in the simulated hydrological variables. The combination of bias correction of the 598

satellite products with ground-based measurements and recalibration of the model parameters 599  
could effectively improve prediction of the hydrological cycle. 600

601

## Acknowledgments 602

We thank the FUI (Fonds Unique Interministériel) HydroSIM project (2018–2021). We also 603

thank the TETFUND for funding P. Datok stay at the Laboratoire Ecologie Fonctionnelle et 604

Environnement, Université de Toulouse. 605

606

## References 607

Abbaspour, K.C., Rouholahnejad, E., Vaghefi, S., Srinivasan, R., Yang, H., and Kløve, B. A., 608  
2015. continental-scale hydrology and water quality model for Europe: Calibration and 609  
uncertainty of a high-resolution large-scale SWAT model. *J. Hydrol.*, 524, 733–752. 610  
<https://doi.org/10.1016/j.jhydrol.2015.03.027> 611

Alsdorf, D., Beighley, E., Laraque, A., Lee, H., Tshimanga, R., O’Loughlin, F., Mahé, G., 612  
Dinga, B., Moukandi, G., and Spencer, R. G. M., 2016. Opportunities for hydrologic 613  
research in the Congo Basin. *Rev. of Geophys.*, 54(2), 378–409. 614  
<https://doi.org/10.1002/2016RG000517> 615

Amorim, J.d.S., Viola, M.R., Junqueira, R., Oliveira, V.A.d., and Mello, C.R.d., 2020. 616  
Evaluation of satellite precipitation products for hydrological modeling in the Brazilian 617  
Cerrado biome. *Water*, 12(9), 2571. <https://doi.org/10.3390/w12092571> 618

Arnold, J.G., Srinivasan, R., Mutiah, R.S., and Williams, J.R., 1998. Large area hydrologic 619  
modeling and assessment part I: Model development. *JAWRA Journal of the American* 620  
*Water Resour. Assoc.*, 34(1), 73–89. <https://doi.org/10.1111/j.1752-1688.1998.tb05961.x> 621

Ashouri, H., Hsu, K.-L., Sorooshian, S., Braithwaite, D.K., Knapp, K.R., Cecil, L.D., Nelson, 622  
B.R., and Prat, O.P., 2015. PERSIANN-CDR: daily precipitation climate data record 623  
from multisatellite observations for hydrological and climate studies. *Bull. Am.* 624  
*Meteorol. Soc.*, 96(1), 69–83. <https://doi.org/10.1175/BAMS-D-13-00068.1> 625

Awange, J., Ferreira, V., Forootan, E., Khandu, Andam-Akorful, S., Agutu, N., He, F., 626  
2016. Uncertainties in remotely sensed precipitation data over Africa. *Int. J. Climatol.*, 36, 627  
303–323. <https://doi.org/10.1002/joc.4346>. 628

Ayehu, G. T., Tadesse, T., Gessesse, B., and Dinku, T., 2018. Validation of new satellite 629  
rainfall products over the Upper Blue Nile Basin, Ethiopia, *Atmos. Meas. Tech.*, 11, 630  
1921–1936. <https://doi.org/10.5194/amt-11-1921-2018> 631

Beck, H.E., van Dijk, A.I., De Roo, A., Miralles, D.G., McVicar, T.R., Schellekens, J., and 632  
Bruijnzeel, L.A., 2016. Global-scale regionalization of hydrologic model parameters. 633  
*Water Resour. Res.*, 52 (5), 3599–3622. <https://doi.org/10.1002/2015WR018247> 634

Beck, H.E., Van Dijk, A.I., Levizzani, V., Schellekens, J., Gonzalez Miralles, D., Martens, B., 635  
and De Roo, A., 2017. MSWEP: 3-hourly 0.25 global gridded precipitation (1979–2015) 636  
by merging gauge, satellite, and reanalysis data. *Hydrol. Earth Syst. Sci.*, 21(1), 589–615. 637  
<https://doi.org/10.5194/hess-21-589-2017> 638

Bultot, F., 1971. Atlas Climatologique du Bassin Congolais : Deuxième partie, les composantes du 639

- bilan d'eau. Publications de L'Institut National pour L'Etude Agronomique du Congo (I.N.E.A.C.). 640  
641
- Cakir, R., Sauvage, S., Gerino, M., Volk, M., and Sanchez-Perez, J.M., 2020. Assessment of 642  
ecological function indicators related to nitrate under multiple human stressors in a 643  
large watershed. *Ecol. Indicat.*, 111, 106016. [https://doi.org/10.1016/j.](https://doi.org/10.1016/j.ecolind.2019.106016) 644  
[ecolind.2019.106016](https://doi.org/10.1016/j.ecolind.2019.106016). 645
- Crowhurst, D., Dadson, S., Peng, J., and Washington R., 2021. Contrasting controls on Congo 646  
Basin evaporation at the two rainfall peaks. *Clim Dyn.*, 56, 1609–1624. 647  
<https://doi.org/10.1007/s00382-020-05547-1> 648
- Datok, P., Fabre, C., Sauvage, S., N'kaya, G.M., Paris, A., Dos Santos, V., Laraque, A., and 649  
Sánchez Pérez, J.-M. 2021. Investigating the role of the Cuvette Centrale in the hydrology 650  
of the Congo River Basin. In: *Congo Basin Hydrology, Climate, and Biogeochemistry: A* 651  
*Foundation for the Future. Geophysical Monograph Series.* Alsdorf, D., Moukandi, G., 652  
Tshimanga, R., Eds. John Wiley & Sons Inc. Hoboken, NJ, USA. 653
- Dos Santos, V., Laurent, F., Abe, C., and Messner, F., 2018. Hydrologic Response 654  
to Land Use Change in a Large Basin in Eastern Amazon. *Water*, 10, 655  
1–19. <https://doi.org/10.3390/w10040429> 656
- BRLi. (2016). Développement et mise en place de l'outil de 657  
modélisation et d'allocation des ressources en eau du Bassin 658  
du Congo: Rapport technique de construction et de calage du 659  
modèle, CICOS, Kinshasa, RDC. <https://www.cicos.int> 660
- Dile, Y. T., and Srinivasan, R., 2014. Evaluation of CFSR climate data for hydrologic 661  
prediction in data- scarce watersheds: An application in the Blue Nile River Basin. *Journal* 662  
*of the American Water Resour. Assoc.*, 50(5), 1226–1241. 663  
<https://doi.org/10.1111/jawr.12182> 664
- Funk, C., Peterson, P., Landsfeld, M., Pedreros, D., Verdin, J., Shukla, S., Husak, G., Rowland, 665  
J., Harrison, L., Hoell, A., and Michaelsen J., 2015. The climate hazards infrared 666  
precipitation with stations - A new environmental record for monitoring extremes. *Sci.* 667  
*Data*, 2, 1–21. <https://doi.org/10.1038/sdata.2015.66> 668
- Galavi, H., and Mirzaei, M., 2020. Analyzing Uncertainty Drivers of Climate Change Impact 669  
Studies in Tropical and Arid Climates. *Water Resour Manage*, 34, 2097–2109. 670  
<https://doi.org/10.1007/s11269-020-02553-0> 671
- Gosset, M., Alcoba, M., Roca, R., Urbani, G., and Cloché, S., 2018. Evaluation of TAPEER 672  
daily estimates and other GPM era products against dense gauge networks in West Africa, 673  
analyzing ground reference uncertainty *Q. J. R. Meteorol. Soc.*, 144, 255–69. 674  
<https://doi.org/10.1002/qj.3335> 675
- Gupta, H.V., Kling, H., Yilmaz, K.K., and Martinez, G.F., 2009. Decomposition of the mean 676  
squared error and NSE performance criteria: Implications for improving hydrological 677  
modelling. *J. Hydrol.*, 377 (1–2), 80–91. <https://doi.org/10.1016/j.jhydrol.2009.08.003> 678
- Harris, N. L., Goldman, E., Gabris, C., Nordling, J., Minnemeyer, S., Ansari, S., Lippmann, 679  
M., Bennett, L., Raad, M., Hansen, M., and Potapov, P., 2017. Using spatial statistics to 680  
identify emerging hot spots of forest loss. *Environ. Res. Lett.*, 12, L024012. 681  
<https://doi.org/10.1088/1748-9326/aa5a2f> 682
- Hou, A. Y., Kakar, R. K., Neeck, S., Azarbarzin, A. A., Kummerow, C. D., Kojima, M., Oki, 683  
R., Nakamura, K., & Iguchi, T. (2014). The Global Precipitation Measurement Mission, 684  
*Bulletin of the American Meteorological Society*, 95(5), 701-722, 685  
<https://doi.org/10.1175/BAMS-D-13-00164.1> 686
- Hua, W., Zhou, L., Nicholson, S.E. Chen, H., and Qin, M., 2019. Assessing reanalysis data for 687  
understanding rainfall climatology and variability over Central Equatorial Africa. *Clim* 688  
*Dyn.*, 53, 651–669. <https://doi.org/10.1007/s00382-018-04604-0> 689

- Huffman, G.J., Adler, R.F., Morrissey, M.M., Bolvin, D.T., Curtis, S., Joyce, R., McGavock, B., and Susskind, J., 2001. Global precipitation at one-degree daily resolution from multisatellite observations. *J. Hydrometeorol.*, 2 (1), 36–50. [https://doi.org/10.1175/1525-7541\(2001\)002<0036:GPAODD>2.0.CO;2](https://doi.org/10.1175/1525-7541(2001)002<0036:GPAODD>2.0.CO;2)
- Huffman, G.J., Bolvin, D.T., Nelkin, E.J., Wolff, D.B., Adler, R.F., Gu, G., Hong, Y., Bowman, K.P., and Stocker, E.F., 2007. The TRMM multisatellite precipitation analysis (TMPA): quasi-global, multiyear, combined-sensor precipitation estimates at fine scales. *J. Hydrometeorol.*, 8 (1), 38–55. <https://doi.org/10.1175/JHM560.1>
- Huffman, G.J., Bolvin, D.T., Braithwaite, D., Hsu, K.L., Joyce, R., Kidd, C., Nelkin, E.J., Sorooshian, S., Tan, J., and Xie, P. 2019. Algorithm Theoretical Basis Document (ATBD) Version 06 NASA Global Precipitation Measurement (GPM) Integrated Multi-satellite Retrievals for GPM (IMERG) ; National Aeronautics and Space Administration (NASA): Washington, DC, USA, pp. 1–34.
- Jackson, Nicholson, S. E., and Klotter, D., 2009. Mesoscale convective systems over western equatorial Africa and their relationship to large-scale circulation. *Mon. Weather Rev.*, 137, 1272–1294. <https://doi.org/10.1175/2008MWR2525.1>
- KGE-hydroGOF, 2017. “Kling–Gupta Efficiency.” <https://www.rforge.net/doc/packages/hydroGOF/KGE.html>
- Kidd, C., and Levizzani, V., 2011. Status of satellite precipitation retrievals, *Hydrol. Earth Syst. Sci.*, 15, 1109–1116, <https://doi.org/10.5194/hess-15-1109-2011>
- Kidd, C., Becker, A., Huffman, G. J., Muller, C. L., Joe, P., Skofronick-Jackson, G., & Kirschbaum, D. B. (2017). So, How Much of the Earth’s Surface Is Covered by Rain Gauges?, *Bulletin of the American Meteorological Society*, 98(1), 69–78, <https://doi.org/10.1175/BAMS-D-14-00283.1>
- Kubota, T., Shige, S., Hashizume, H., Aonashi, K., Takahashi, N., Seto, S., Hirose, M., Takayabu, Y. N., Ushio, T., Nakagawa, K., Iwanami, K., Kachi, M. and Okamoto, K., 2007. Global Precipitation Map Using Satellite-Borne Microwave Radiometers by the GSMaP Project: Production and Validation, *IEEE 5 Trans. Geosci. Remote Sens.*, 45(7), 2259–2275, <https://doi.org/10.1109/tgrs.2007.895337>.
- Laraque, A., Mahé, G., Orange, D. and Marieu, B., 2001. Spatiotemporal variations in hydrological regimes within Central Africa during the XXth century. *J. Hydrol.*, 245(1–4), 104–117. [https://doi.org/10.1016/S0022-1694\(01\)00340-7](https://doi.org/10.1016/S0022-1694(01)00340-7)
- Loucks, D. P. and Van Beek, E., 2017. An Introduction to Probability, Statistics, and Uncertainty, in: *Water Resource Systems Planning and Management*, 51–72, Springer, Cham, 2017. <https://doi.org/10.1007/978-3-319-44234-1>
- Maggioni, V., Massari, C., 2018. On the performance of satellite precipitation products in riverine flood modeling: a review. *J. Hydrol.*, 558, 214–224. <https://doi.org/10.1016/j.jhydrol.2018.01.039>
- Maidment, R. I., Grimes, D., Black, E., Tarnavsky, E., Young, M., Greatrex, H., Allan, R. P., Stein, T., Nkonde, E., Senkunda, S. and Alcántara, E. M. U., 2017. A new, long-term daily satellite-based rainfall dataset for operational monitoring in Africa. *Sci. Data.*, 4, 1–19. <https://doi.org/10.1038/sdata.2017.63>
- Mandal, U., Sena, D.R., Dhar, A., Panda, S.N., Adhikary, P.P., Mishra, P.K., 2021. Assessment of climate change and its impact on hydrological regimes and biomass yield of a tropical river basin. *Ecol. Ind.*, 126, 107646. <https://doi.org/10.1016/j.ecolind.2021.107646>
- McCollum, J. R., Gruber A., and Ba M. B., 2000. Discrepancy between gauges and satellite estimates of rainfall in equatorial Africa. *J. Appl. Meteor.*, 39, 666–679. <https://doi.org/10.1175/1520-0450-39.5.666>
- Melaku, N. D., and Wang, J., 2019. A modified SWAT module for estimating groundwater table at Lethbridge and Barons, Alberta, Canada. *J. Hydrol.*, 575, 420–431.

<a href="https://doi.org/10.1016/j.jhydrol.2019.05.052">https://doi.org/10.1016/j.jhydrol.2019.05.052</a>	740
Moriasi, D.N., Arnold, J.G., van Liew, M.W., Bingner, R.L., Harmel, R.D., Veith, T.L., 2007. Model evaluation guidelines for systematic quantification of accuracy in watershed simulations. <i>Trans. ASABE</i> 50, 885–900. <a href="https://doi.org/10.13031/2013.23153">https://doi.org/10.13031/2013.23153</a>	741 742 743
Moriasi, D.N., Gitau, M.W., Pai, N., Daggupati, P., 2015. Hydrologic and water quality models: performance measures and evaluation criteria. <i>Trans. ASABE</i> 58, 1763–1785. <a href="https://doi.org/10.13031/trans.58.10715">https://doi.org/10.13031/trans.58.10715</a>	744 745 746
Moukandi N’kaya, G. D., Laraque, A., Paturol, J. M, Gulemvuga, G., Mahé, G., and Tshimanga Muamba, R. (2021). A new look at hydrology in the Congo Basin, based on the study of multi- decadal chronicles. In: Alsdorf, D., Tshimanga Muamba, R., and Moukandi N’kaya, G. D. (Eds.), <i>Congo Basin Hydrology, Climate, and Biogeochemistry: A Foundation for the Future</i> , AGU Geophysical Monograph Series. Hoboken, NJ: John Wiley & Sons, Inc.	747 748 749 750 751 752
Munzimi, Y.A., Hansen, M.C., Adusei, B. and Senay, G.B., 2015. Characterizing Congo basin rainfall and climate using Tropical Rainfall Measuring Mission (TRMM) satellite data and limited rain gauge ground observations. <i>J. Appl. Meteorol. Climatol.</i> , 54, 541–555. <a href="https://doi.org/10.1175/JAMC-D-14-0052.1">https://doi.org/10.1175/JAMC-D-14-0052.1</a>	753 754 755 756
Nash, J.E. and Sutcliffe, J.V., 1970. River Flow Forecasting through Conceptual Model. Part 1-A Discussion of Principles. <i>J. Hydrol.</i> , 10, 282-290. <a href="http://dx.doi.org/10.1016/0022-1694(70)90255-6">http://dx.doi.org/10.1016/0022-1694(70)90255-6</a>	757 758 759
Negron Juarez, R. I. N., Li, W. H., Fu, R., Fernandes, K., and Cardoso, A. D., 2009. Comparison of precipitation datasets over the tropical South American and African continents. <i>J. Hydrometeor.</i> , 10, 289–299. <a href="https://doi.org/10.1175/2008JHM1023.1">https://doi.org/10.1175/2008JHM1023.1</a>	760 761 762
Nicholson, S. E., Klotter, D., Zhou, L., and Hua, W., 2019. Validation of Satellite Precipitation Estimates over the Congo Basin. <i>J. Hydrometeorol.</i> , 20(4), 631-656, <a href="https://doi.org/10.1175/JHM-D-18-0118.1">https://doi.org/10.1175/JHM-D-18-0118.1</a>	763 764 765
Novella, N.S. and Thiaw, W.M., 2013. African Rainfall Climatology Version 2 for Famine Early Warning Systems. <i>J. Appl. Meteorol. Climatol.</i> , 52, 588-606. <a href="https://doi.org/10.1175/JAMC-D-11-0238.1">https://doi.org/10.1175/JAMC-D-11-0238.1</a>	766 767 768
Oliveira, R.; Maggioni, V.; Vila, D.; Morales, C. Characteristics and Diurnal Cycle of GPM Rainfall Estimates over the Central Amazon Region. <i>Remote Sens.</i> 2016, 8, 544. <a href="https://doi.org/10.3390/rs8070544">https://doi.org/10.3390/rs8070544</a>	769 770 771
Peng, J., Liu, T., Huang, Y., Ling, Y., Li, Z., Bao, A., Chen, X., Kurban, A., and De Maeyer, P., 2021. Satellite-Based Precipitation Datasets Evaluation Using Gauge Observation and Hydrological Modeling in a Typical Arid Land Watershed of Central Asia. <i>Remote Sens.</i> , 13, 221. <a href="https://doi.org/10.3390/rs13020221">https://doi.org/10.3390/rs13020221</a>	772 773 774 775
Roca, R. Estimation of extreme daily precipitation thermodynamic scaling using gridded satellite precipitation products over tropical land. <i>Environ. Res. Lett.</i> , IOP Publishing, 2019, 14. <a href="https://doi.org/10.1088/1748-9326/ab35c6">https://doi.org/10.1088/1748-9326/ab35c6</a>	776 777 778
Roca, R., Alexander, L. V., Potter, G., Bador, M., Jucá, R., Contractor, S., Bosilovich, M. G., and Cloché, S., 2019. FROGS: a daily 1° × 1° gridded precipitation database of rain gauge, satellite and reanalysis products, <i>Earth Syst. Sci. Data</i> , 11, 1017–1035. <a href="https://doi.org/10.5194/essd-11-1017-2019">https://doi.org/10.5194/essd-11-1017-2019</a>	779 780 781 782
Roca, R., Chambon, P., Jobard, I., Kirstetter, P., Gosset, M., & Bergès, J. C. (2010). Comparing Satellite and Surface Rainfall Products over West Africa at Meteorologically Relevant Scales during the AMMA Campaign Using Error Estimates, <i>Journal of Applied Meteorology and Climatology</i> , 49(4), 715-731. <a href="https://doi.org/10.1175/2009JAMC2318.1">https://doi.org/10.1175/2009JAMC2318.1</a>	783 784 785 786 787
Runge, J., 2007. The Congo River, Central Africa, in <i>Large Rivers: Geomorphology and Management</i> . In: Large Rivers. Gupta, A., Ed. 293-309, Wiley, U.K.	788 789

<a href="https://doi.org/10.1002/9780470723722.ch14">https://doi.org/10.1002/9780470723722.ch14</a>	790
Satgé, F. D., Defrance, B. S., Bonnet, M.P., Seyler, F., Rouché, N., Pierron, F., and Paturol, J.E., 2020. Evaluation of 23 gridded precipitation datasets across West Africa. <i>J. Hydrol.</i> , 581, 124412. <a href="https://doi.org/10.1016/j.jhydrol.2019.124412">https://doi.org/10.1016/j.jhydrol.2019.124412</a>	791 792 793
Shao, G., Guan, Y., Zhang, D., Yu, B., and Zhu, J., 2018. The Impacts of Climate Variability and Land Use Change on Streamflow in the Hailutu River Basin. <i>Water</i> , 10, 814. <a href="https://doi.org/10.3390/w10060814">https://doi.org/10.3390/w10060814</a>	794 795 796
Sharannya, T.M., Al-Ansari, N., Deb Barma, S., and Mahesha, A., 2020. Evaluation of Satellite Precipitation Products in Simulating Streamflow in a Humid Tropical Catchment of India Using a Semi-Distributed Hydrological Model. <i>Water</i> , 12, 2400. <a href="https://doi.org/10.3390/w12092400">https://doi.org/10.3390/w12092400</a>	797 798 799 800
Skofronick-Jackson, G., Petersen, W.A., Berg, W., Kidd, C., Stocker, E.F., Kirschbaum, D.B., Kakar, R., Braun, S.A., Huffman, G.J., Iguchi, T., Kirstetter, P.E., Kummerow, C., Meneghini, R., Oki, R., Olson, W.S., Takayabu, Y.N., Kurukawa, K. and Wilheit, T. (2017) The Global Precipitation Measurement (GPM) mission for science and society. <i>Bulletin of the American Meteorological Society</i> , 98, 1679–1695. <a href="https://doi.org/10.1175/BAMS-D-15-00306.1">https://doi.org/10.1175/BAMS-D-15-00306.1</a>	801 802 803 804 805 806
Sok, T., Oeurng, C., Ich, I., Sauvage, S., and Sánchez-Pérez, J. M., 2020. Assessment of Hydrology and Sediment Yield in the Mekong River Basin Using SWAT Model. <i>Water</i> , 12, 3503. <a href="https://doi.org/10.3390/w12123503">https://doi.org/10.3390/w12123503</a>	807 808 809
Strauch, M., and Volk, M., 2013. SWAT plant growth modification for improved modeling of perennial vegetation in the tropics. <i>Ecol. Model.</i> , 269, 98–112. <a href="https://doi.org/10.1016/j.ecolmodel.2013.08.013">https://doi.org/10.1016/j.ecolmodel.2013.08.013</a>	810 811 812
Sun, Q., Miao, C., Duan, Q., Ashouri, H., Sorooshian, S., and Hsu, K. L. 2018. A review of global precipitation datasets: data sources, estimation, and intercomparisons. <i>Rev. Geophys.</i> , 56, 79–10. <a href="https://doi.org/10.1002/2017RG000574">https://doi.org/10.1002/2017RG000574</a>	813 814 815
Tan, M.L., and Yang, X., 2020. Effect of rainfall station density, distribution and missing values on SWAT outputs in tropical region. <i>J. Hydrol.</i> , 584 (2020), 124660. <a href="https://doi.org/10.1016/j.jhydrol.2020.124660">https://doi.org/10.1016/j.jhydrol.2020.124660</a>	816 817 818
Tan, M.L., Samat, N., Chan, N.W., and Roy, R., 2018. Hydro-meteorological assessment of three GPM satellite precipitation products in the Kelantan River Basin, Malaysia. <i>Remote Sens.</i> , 10, 1011. <a href="https://doi.org/10.3390/rs10071011">https://doi.org/10.3390/rs10071011</a>	819 820 821
Tshimanga, R.M., and Hughes, D.A., 2012. Climate change and impacts on the hydrology of the Congo Basin: The case of the northern sub-basins of the Oubangui and Sangha Rivers. <i>Phys. Chem. Earth, Parts A/B/C</i> , 50–52, 72–83. <a href="https://doi.org/10.1016/j.pce.2012.08.002">https://doi.org/10.1016/j.pce.2012.08.002</a>	822 823 824
Tuo, Y., Duan, Z., Disse, M., and Chiogna, G., 2016. Evaluation of precipitation input for SWAT modeling in Alpine catchment: a case study in the Adige river basin (Italy). <i>Sci. Total Environ.</i> , 573, 66–82. <a href="https://doi.org/10.1016/j.scitotenv.2016.08.034">https://doi.org/10.1016/j.scitotenv.2016.08.034</a>	825 826 827
USDA Soil Conservation Service. <i>National Engineering Handbook; Section 4, Hydrology, Chapter 21; USDA Soil Conservation Service: Washington, DC, USA, 1972.</i>	828 829
Wang, Q., Xia, J., She, D., Zhang, X. Liu, J., and Zhang, Y., 2021. Assessment of four latest long-term satellite-based precipitation products in capturing the extreme precipitation and streamflow across a humid region of southern China. <i>Atmos. Res.</i> , 257 ,105554, <a href="https://doi.org/10.1016/j.atmosres.2021.105554">10.1016/j.atmosres.2021.105554</a>	830 831 832 833
Wei, X., Sauvage, S., Le, T.P.Q., Ouillon, S., Orange, D., Vinh, V.D., and Sanchez-Perez, J.M. 2019. A Modeling Approach to Diagnose the Impacts of Global Changes on Discharge and Suspended Sediment Concentration within the Red River Basin. <i>Water</i> , 11, 958. <a href="https://doi.org/10.3390/w11050958">https://doi.org/10.3390/w11050958</a>	834 835 836 837
Williams, J. R. Flood routing with variable travel time or variable storage coefficients. <i>Trans. ASABE</i> 1969, 12, 100-0103. <a href="https://doi.org/10.13031/2013.38772">https://doi.org/10.13031/2013.38772</a>	838 839

Winchell, M.; Srinivasan, R.; Di Luzio, M.; and Arnold, J.G. Arcswat Interface for SWAT2012: User's Guide; Blackland Research Center, Texas AgriLife Research: Temple, TX, USA, 2013. 840  
841  
842

Xie, P., Joyce, R., Wu, S., Yoo, S.H., Yarosh, Y., Sun, F., and Lin, R. 2017. Reprocessed, bias-corrected CMORPH global high-resolution precipitation estimates from 1998. *J. Hydrometeorol.*, 18, 1617–1641. <https://doi.org/10.1175/JHM-D-16-0168.1> 843  
844  
845

Yin, X., and Gruber, A., 2010. Validation of the abrupt change in GPCP precipitation in the Congo River Basin. *Int. J. Climatol.*, 30(1), 110– 119. <https://doi.org/10.1002/joc.1875> 846  
847

Yin, X., Gruber, A., and Arkin P., 2004. Comparison of the GPCP and CMAP merged gauge–satellite monthly precipitation products for the period 1979–2001. *J. Hydrometeorol.*, 5(6), 1207– 1222. . <https://doi.org/10.1175/JHM-392.1> 848  
849  
850

Zhou, L., Tian, Y., Myneni, R., Ciais, P., Saatchi, S., Liu, Y. Y., Piao, S., Chen, H. Vermote, E. F., Song, C., and Hwang, T., 2014. Widespread decline of Congo rainforest greenness in the past decade. *Nature*, 509, 86–90. <https://doi.org/10.1038/nature13265>. 851  
852  
853  
854  
855  
856  
857  
858  
859  
860  
861  
862  
863  
864  
865  
866  
867  
868  
869  
870  
871  
872

	873
<b>Figure and table captions</b>	874
	875
<b>Figure 1.</b> Congo sub-basins studied. Also, the locations of gauge stations used in this study.	876
	877
<b>Figure 2.</b> The spatial distribution of a) unconditional annual mean and b) 99 <sup>th</sup> percentile of daily accumulated precipitation (in mm/day) during the period from 2001 to 2012 over Congo by the 3B42_v7.0 product from 1°/daily FROGS database.	878
	879
	880
	881
<b>Figure 3.</b> Annual cycle of precipitation (in mm/month) during the period from 2001 to 2012 over the five Congo sub-basins from FROGS database. Dots and lines represent the monthly accumulated medians of each satellite-based precipitation product. Gray shading indicates the 30th and 70th percentile ranges. Satellite-only (gauge-calibrated satellite) precipitation products are represented by dashed (solid) lines.	882
	883
	884
	885
	886
	887
<b>Figure 4.</b> Cumulative probability density functions of occurrence (dashed lines) and amount (solid lines) of daily precipitation during the period from 2001 to 2012 over the five Congo sub-basins from FROGS database. Satellite-only (gauge-calibrated satellite) precipitation products are represented at left (right) panels.	888
	889
	890
	891
	892
<b>Figure 5.</b> Monthly observed and simulated streamflow at gauge stations (a) Brazzaville/Kinshasa (outlet), (b) Lualaba/Kisangani, (c) Kasai/Kutu-Moke, (d) Sangha/Ouesso, and (e) Ubangi/Bangui.	893
	894
	895
	896



**Figure 6.** Relative error between observed and simulated streamflow (Relative error =  $(Q_{sim} - Q_{obs})/Q_{obs}$ ) at gauge stations (a) Brazzaville/Kinshasa (outlet), (b) Lualaba/Kisangani, (c) Kasai/Kutu-Moke, (d) Sangha/Ouesso, and (e) Ubangi/Bangui.

**Figure 7.** Simulated streamflow (in  $m^3/s$ ) hydrographs during the period from 2003 to 2012 for gauges stations: Brazzaville/Kinshasa (outlet), Kasai/Kutu-Moke, Lualaba/Kisangani, Sangha/Ouesso and Ubangi/Bangui. Dots and Lines represent the monthly streamflow of each satellite-based precipitation product. Satellite-only (gauge-calibrated satellite) precipitation products are represented by dashed (solid) lines.

**Figure 8.** Heat map statistical analysis (KGE and PBIAS) of the streamflow simulation results of the selected satellite-based precipitation product. The statistical analysis was calculated using the streamflow from base scenario (3B42\_v7.0) as reference.

**Figure 9.** Simulated annual cycle of evapotranspiration (in mm/month) during the period from 2003 to 2012. Dots and lines represent the monthly accumulated medians of each satellite-based precipitation product. Satellite-only (gauge-calibrated satellite) precipitation products are represented by dashed (solid) lines.

**Figure 10.** Simulated annual cycle of surface runoff (in mm/month) during the period from 2003 to 2012. Dots and lines represent the monthly accumulated medians of each satellite-based precipitation product. Satellite-only (gauge-calibrated satellite) precipitation products are represented by dashed (solid) lines.

**Figure 11.** Simulated annual cycle of soil water content (in mm/month) during the period from 2003 to 2012. Dots and lines represent the monthly accumulated medians of each satellite-based precipitation product. Satellite-only (gauge-calibrated satellite) precipitation products are represented by dashed (solid) lines.

**Table 1.** Summary of the selected satellite-based precipitation products used in the present study. \* Multiple platforms and # Single platform.

**Table 2.** Description of the nature and source of datasets employed in the SWAT Model

**Table 3.** SWAT model performance for predicting monthly streamflow

**Table 4.** Summary of various hydrological studies utilizing satellite-based precipitation products run with the SWAT model

Figure 1.

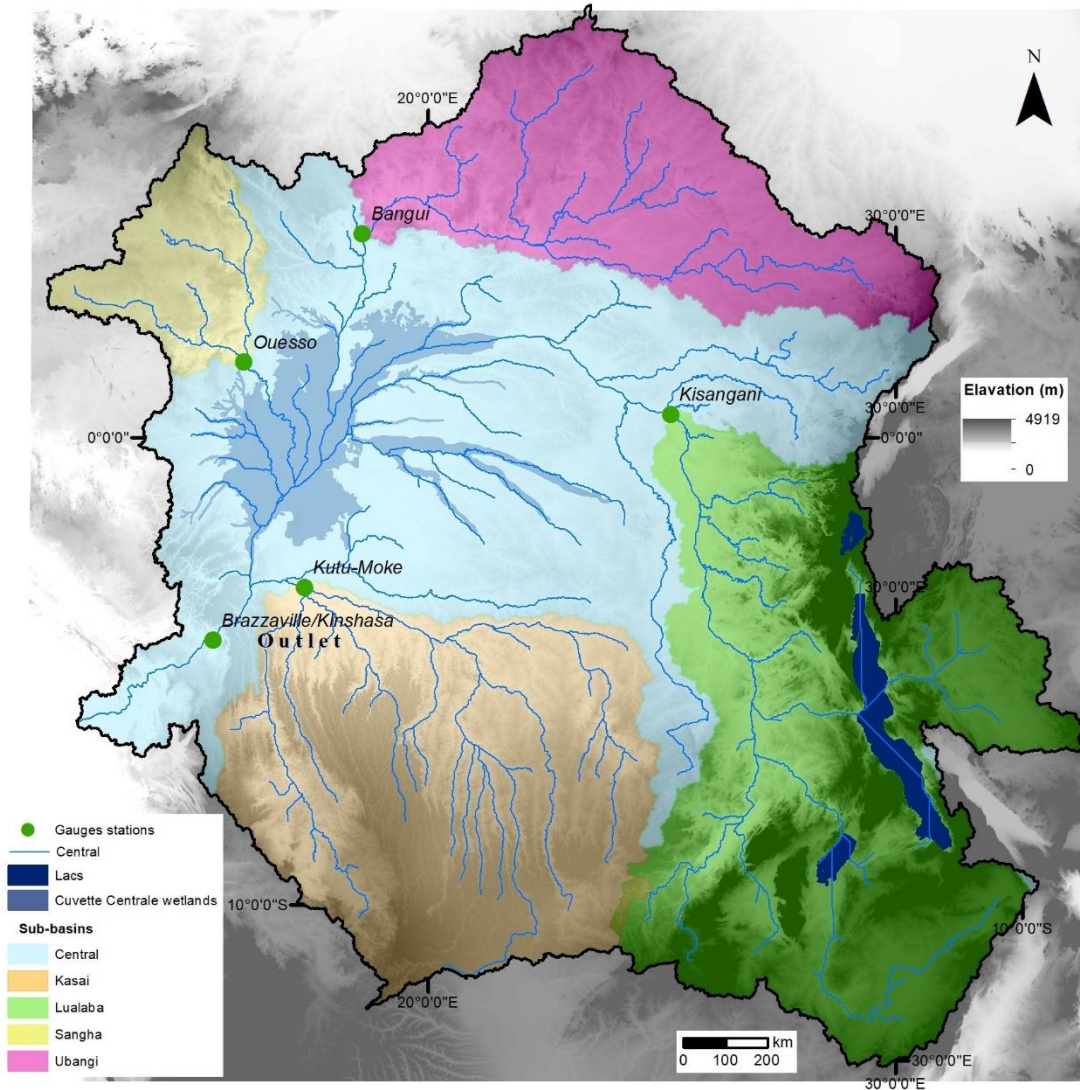
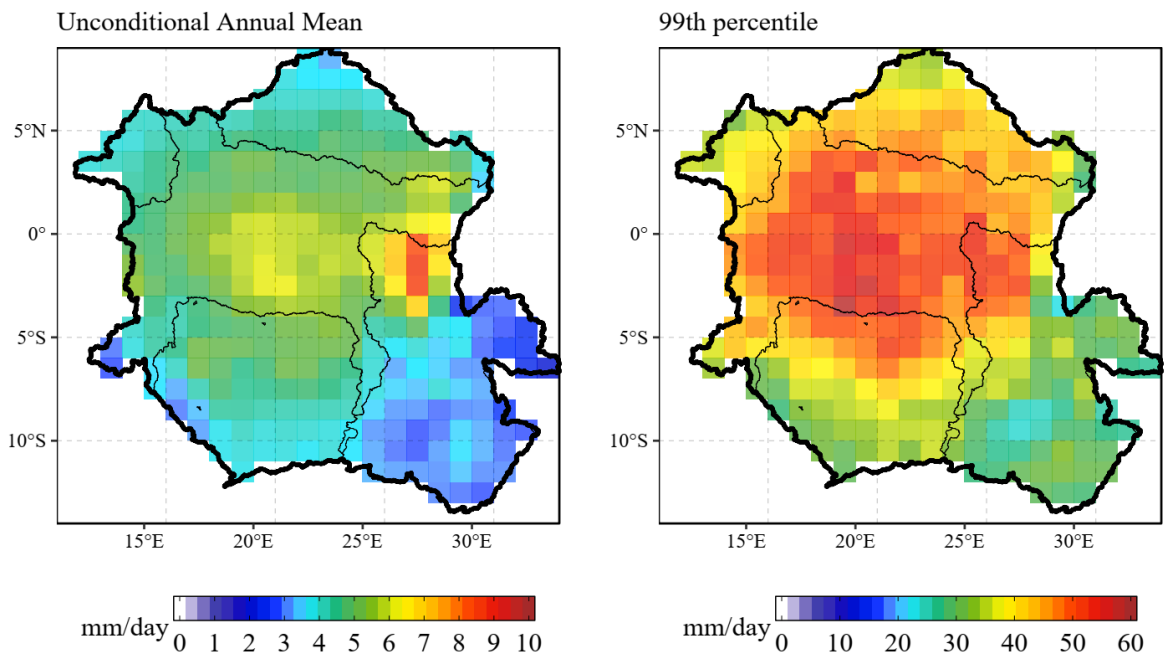


Figure 2.

958



959

960

Figure 3.

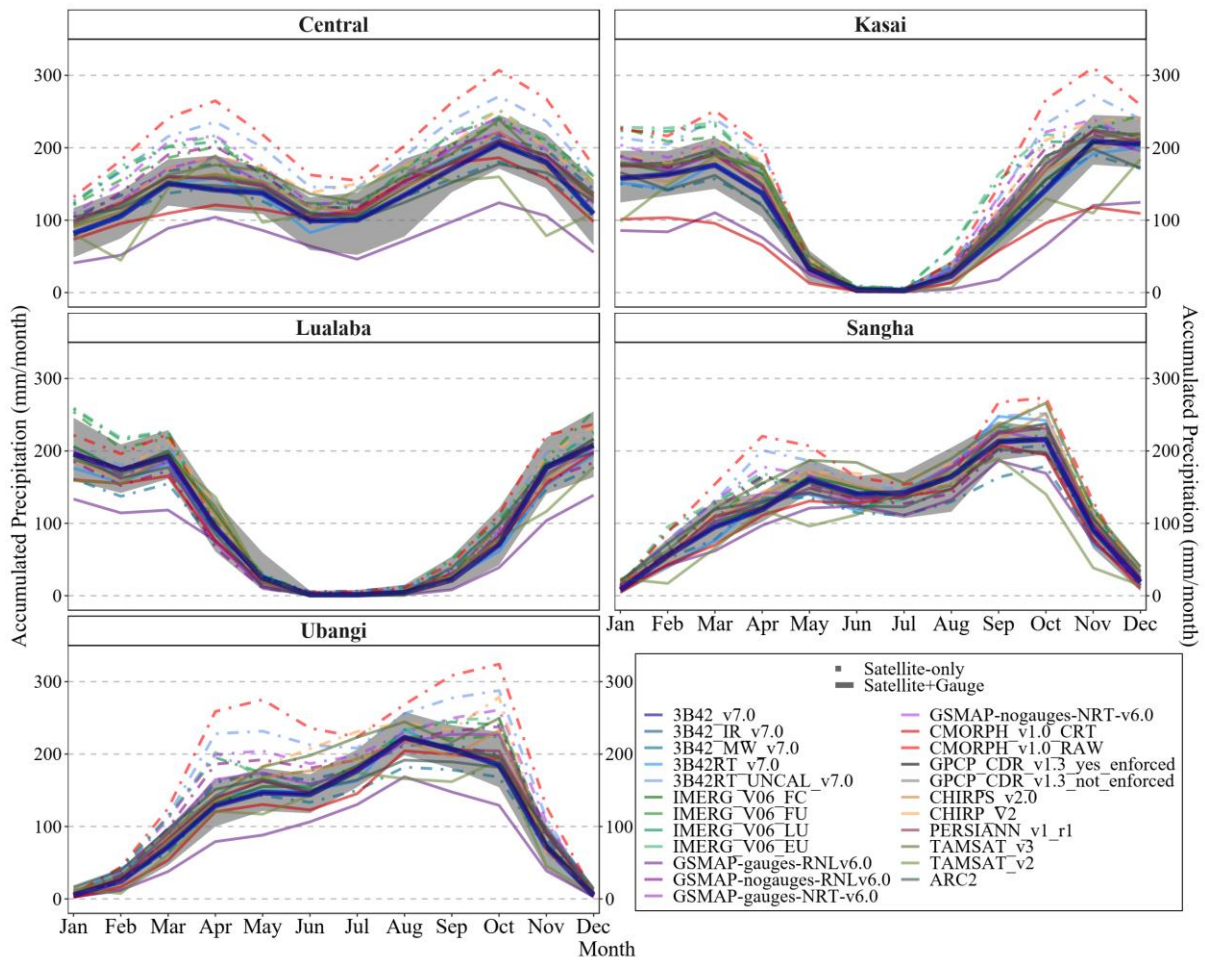
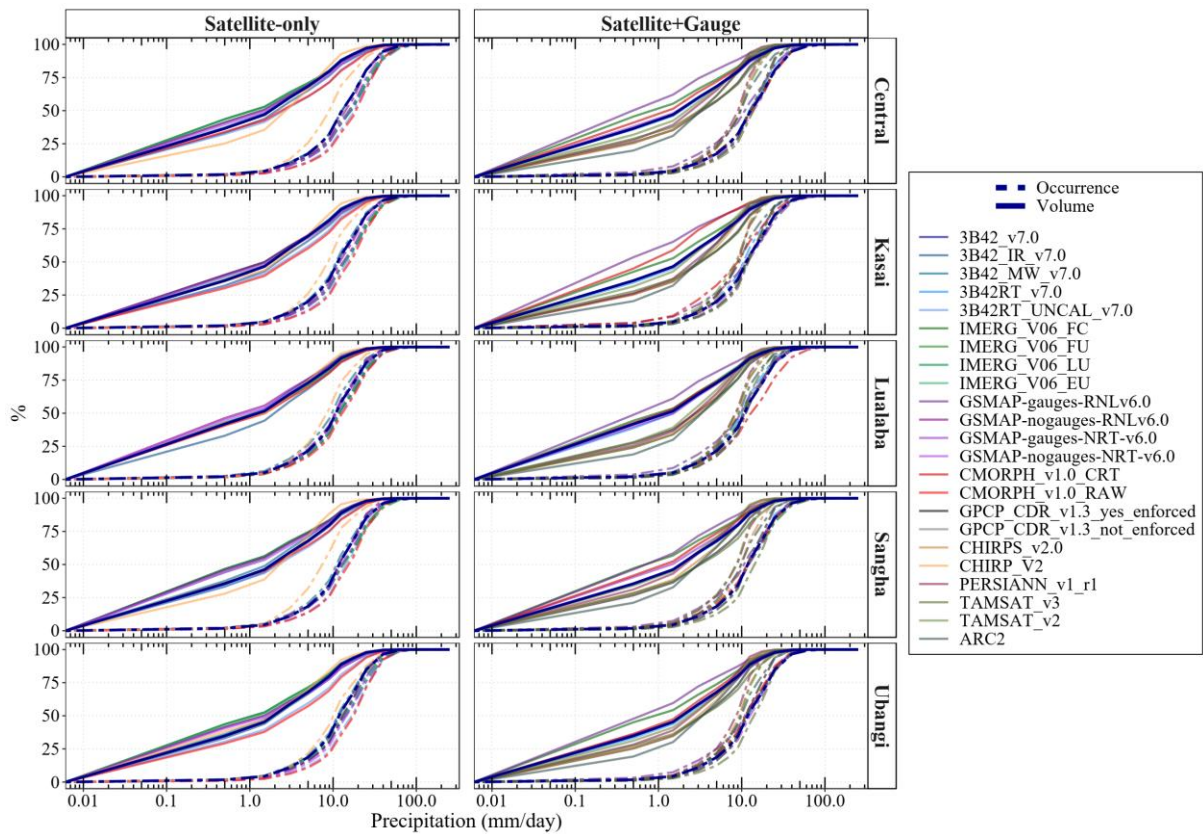


Figure 4.



965

966

967

968

969

970

971

972

973

974

975

976

977

Figure 5.

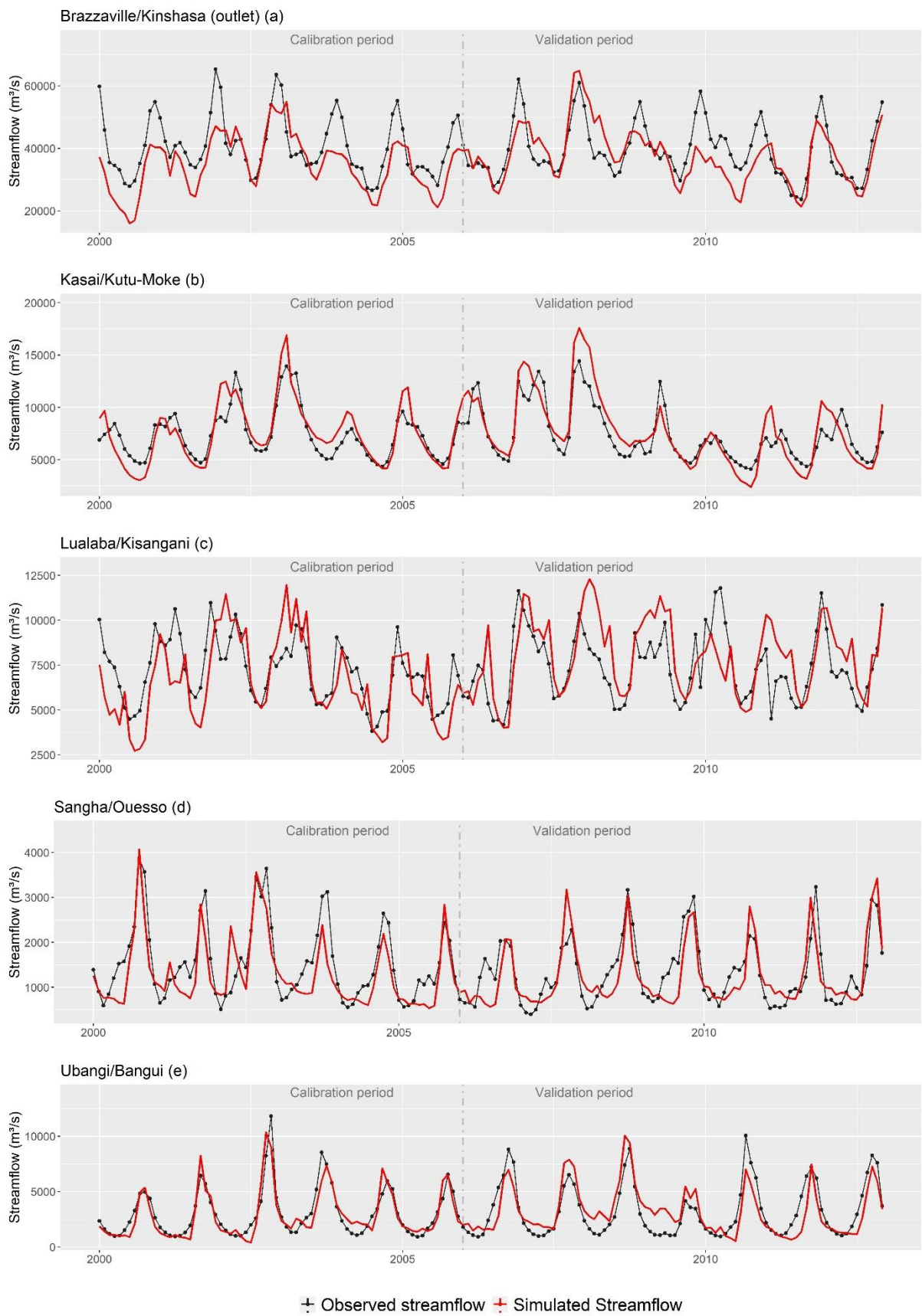
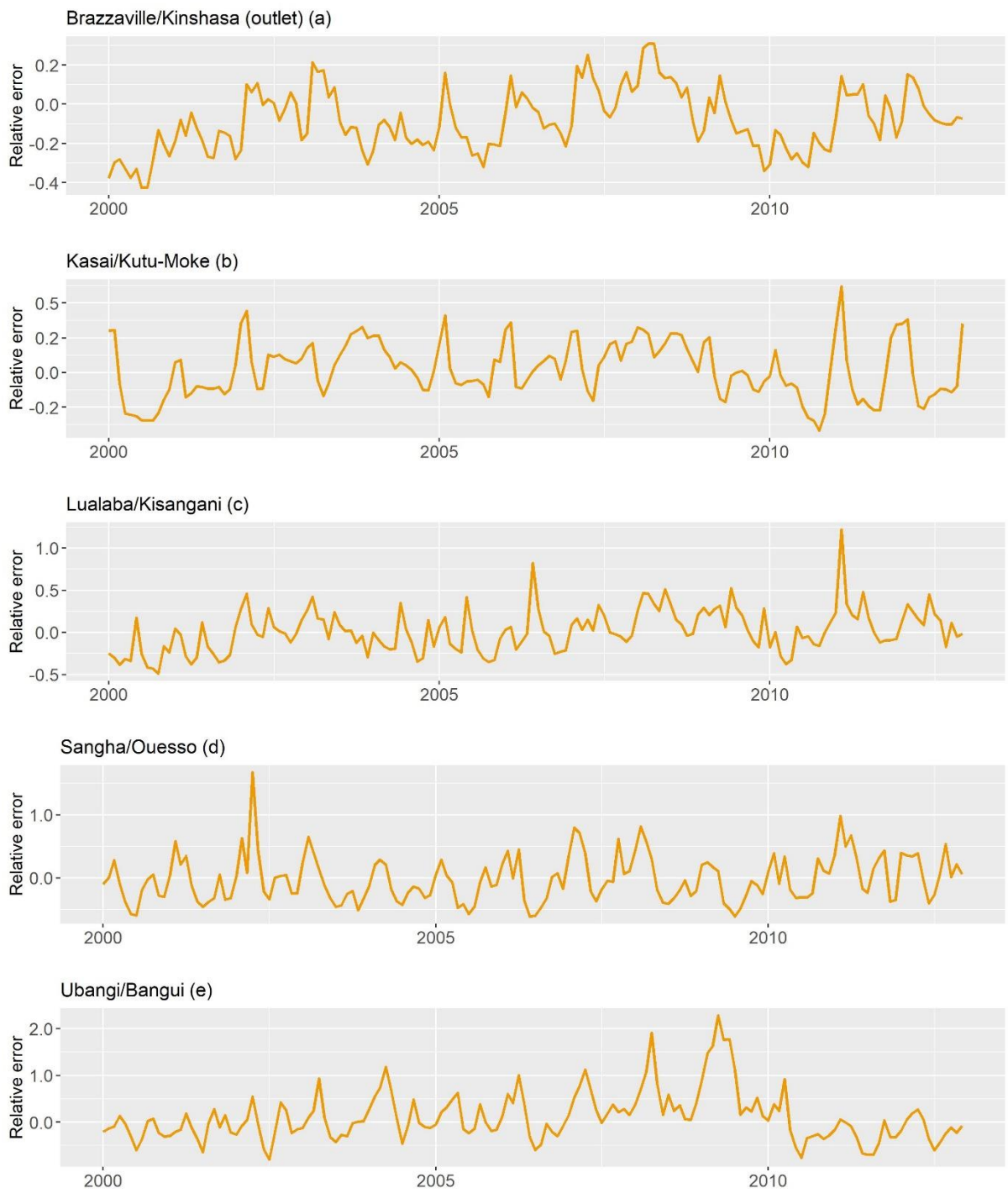


Figure 6.



981

982

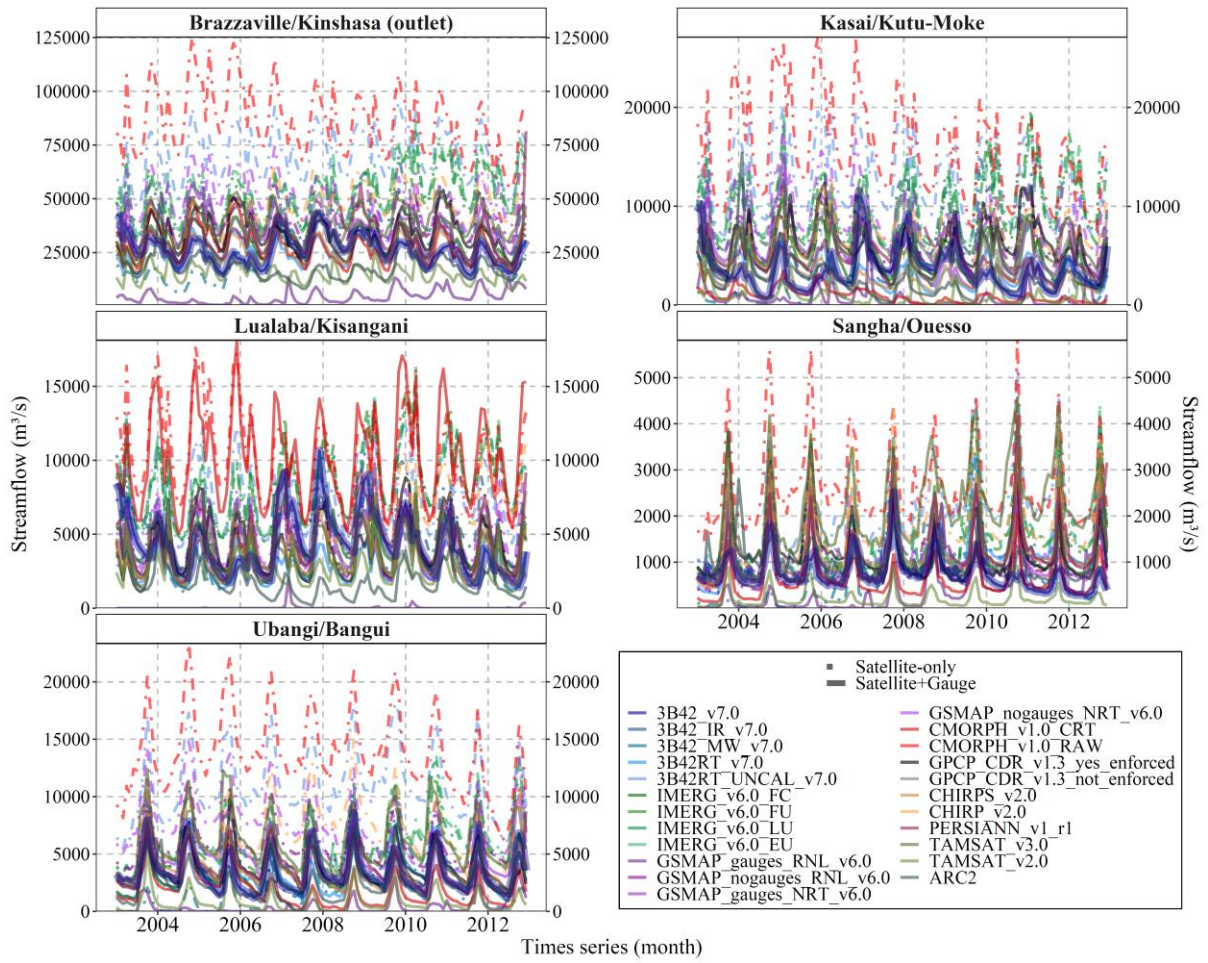
983

984

985



Figure 7.



987

988

989

990

991

992

993

994

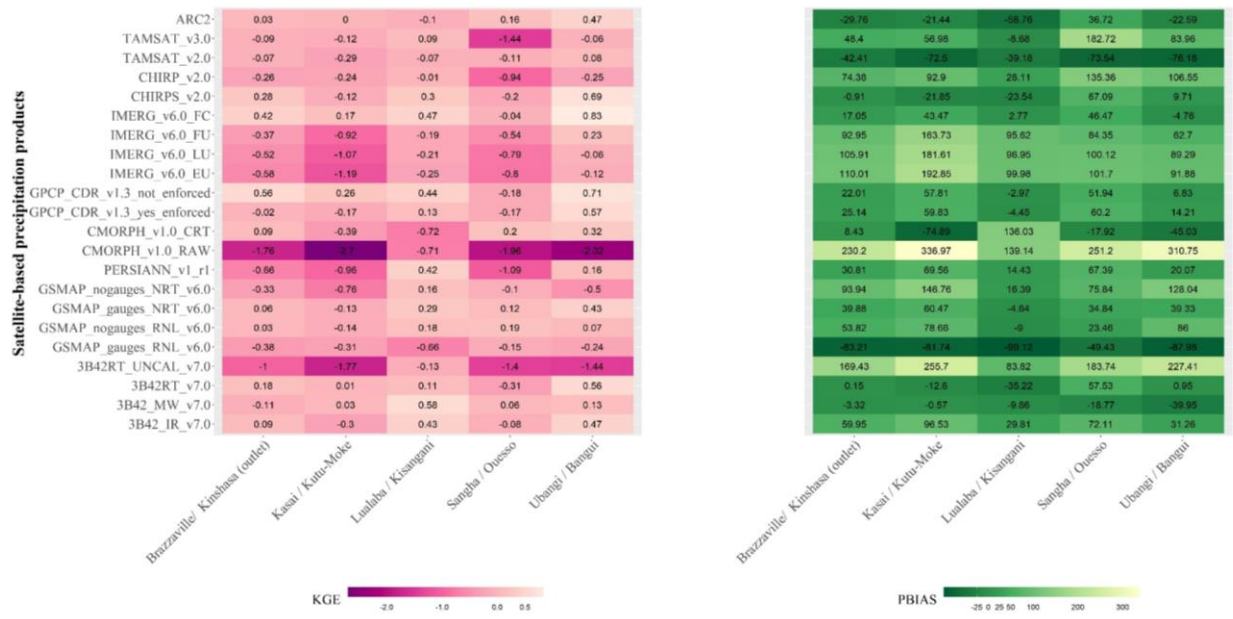
995

996

997

998

Figure 8.



.000

1001

1002

1003

1004

1005

1006

1007

1008

1009

1010

1011

1012

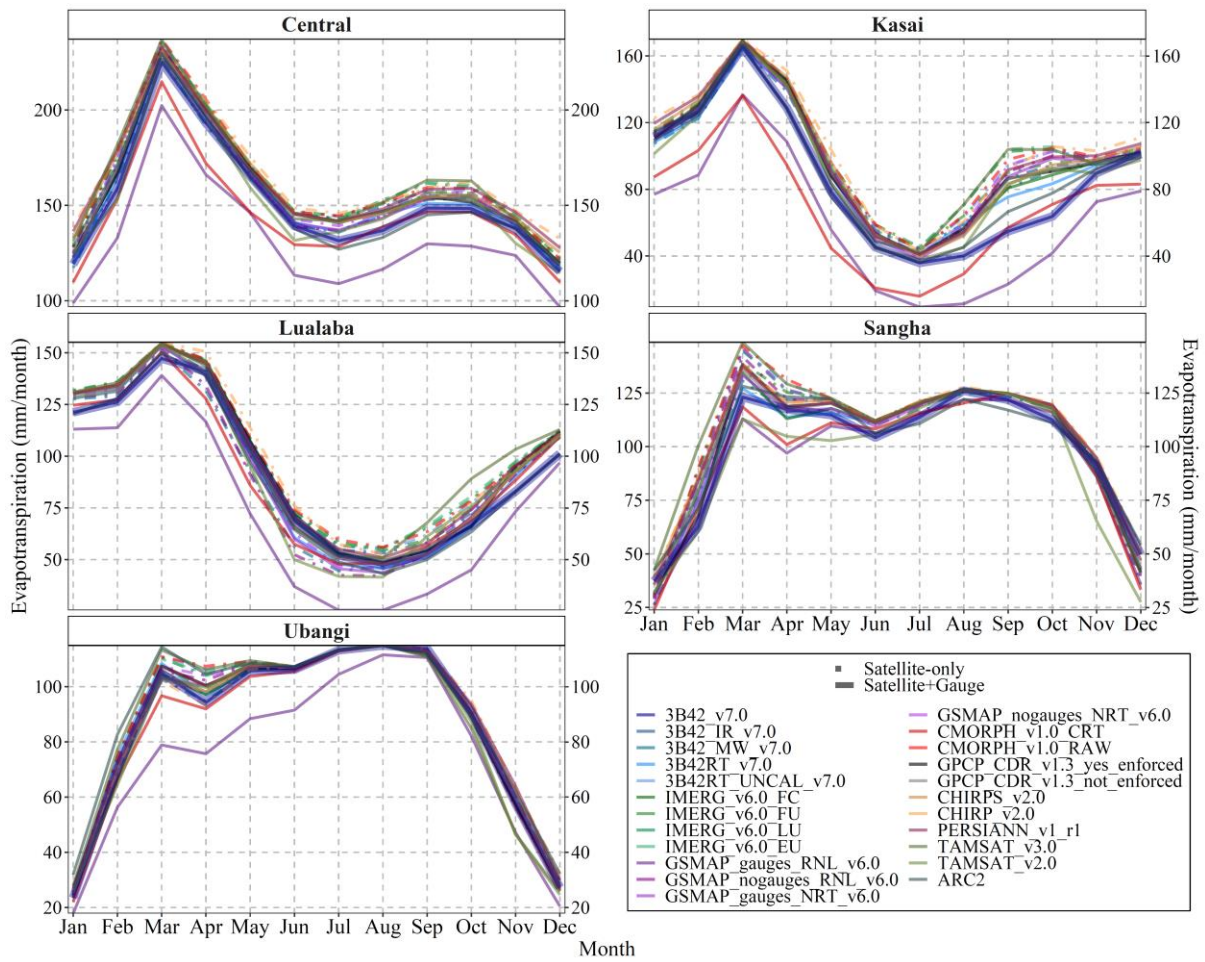
1013

1014

1015

Figure 9.

1016



1017

1018

1019

1020

1021

1022

1023

1024

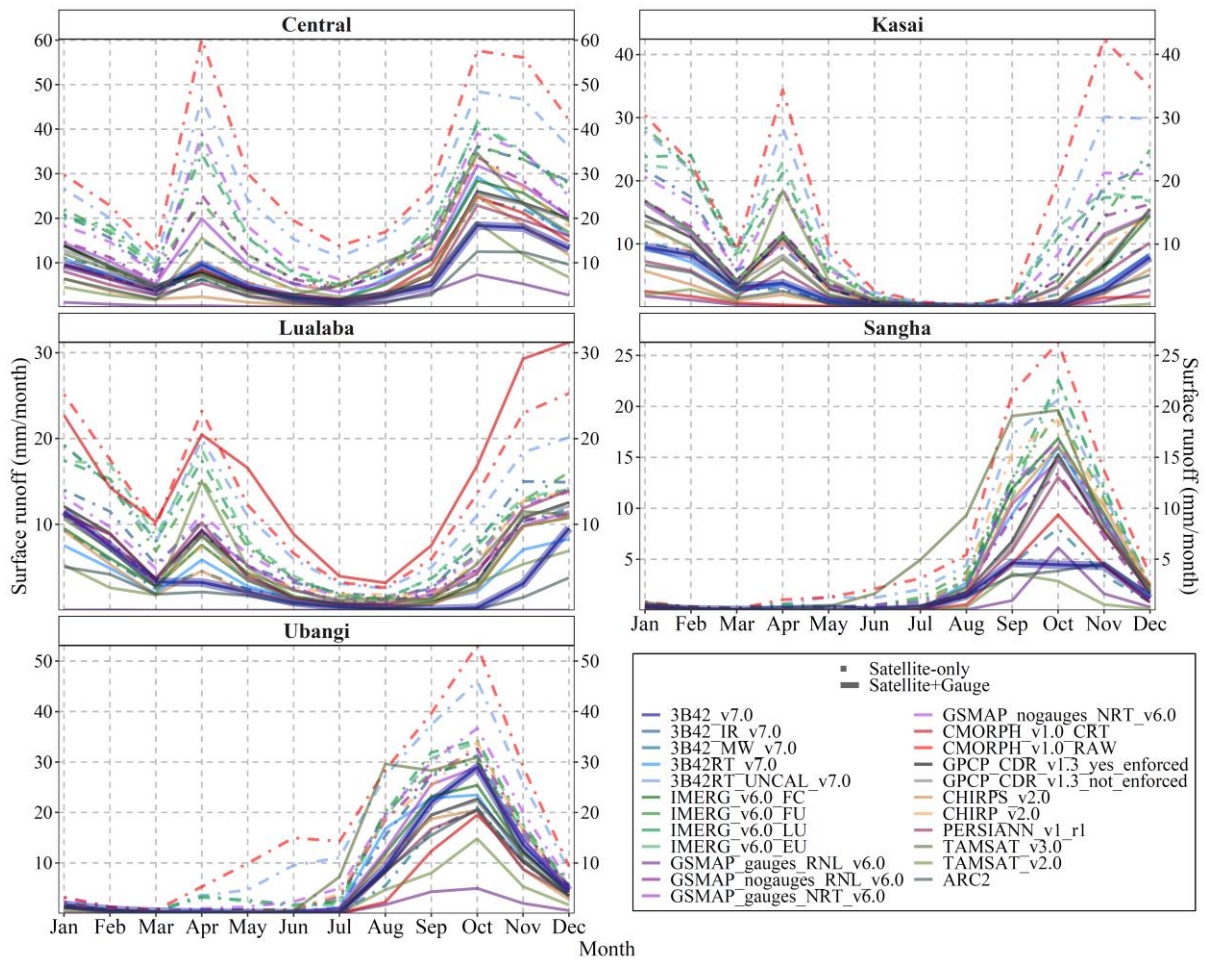
1025

1026

1027

1028

Figure 10.



1030

1031

1032

1033

1034

1035

1036

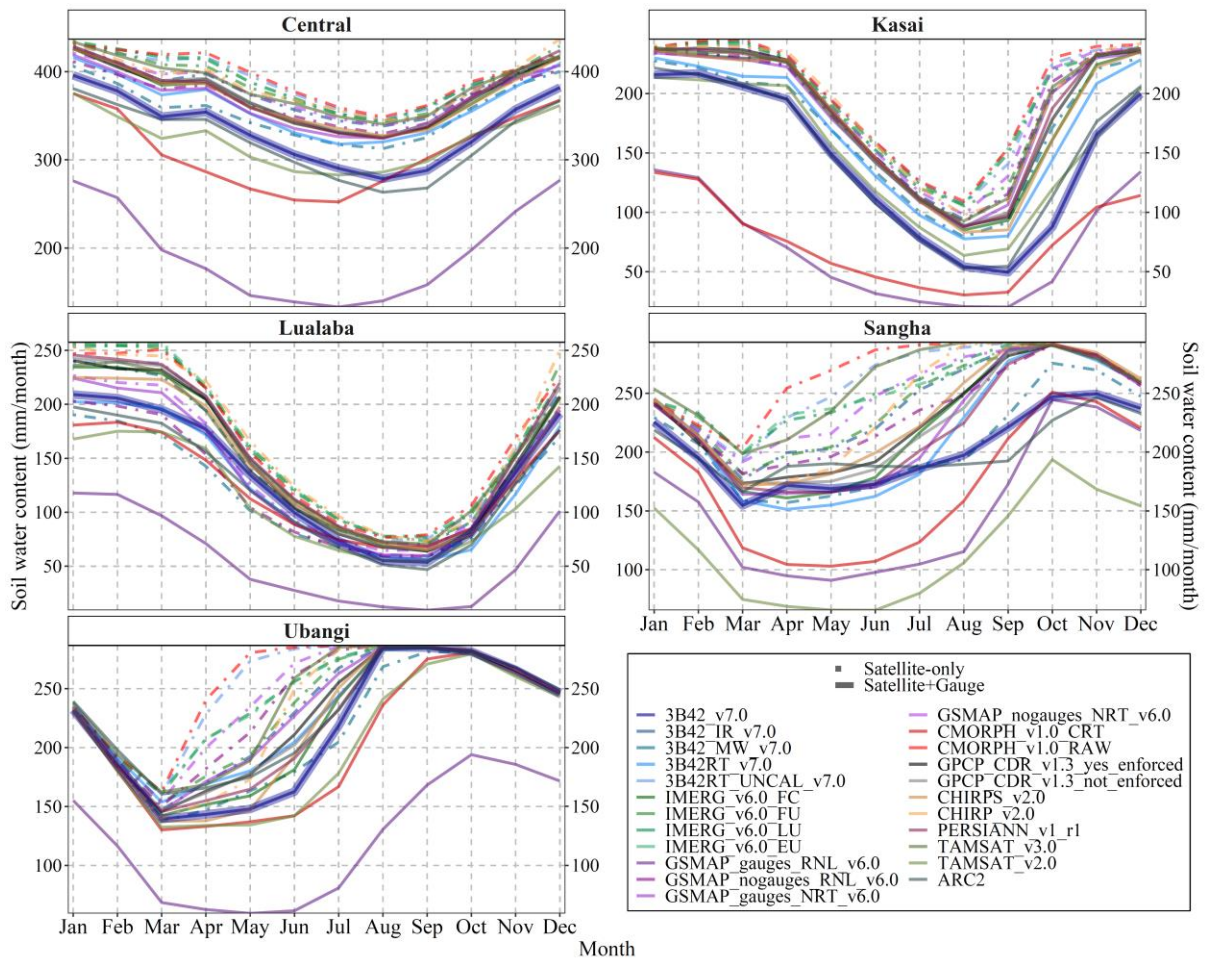
1037

1038

1039

Figure 11.

1040



1041

1042

1043

1044

1045

1046

1047

1048

1049

1050

1051

1052

Table 1.

Type of data	Satellite source	#	Product short name and version	Temporal coverage	Spatial coverage	Reference
Satellite-only (10)	IR+MW*	1	IMERG v6.0 - Early	2000-2018	60° N-S	Huffman et al. (2019)
	IR+MW*	2	IMERG v6.0 - Late	2000-2018	60° N-S	Huffman et al. (2019)
	IR+MW*	3	IMERG V06 - Final Uncal	2000-2018	60° N-S	Huffman et al. (2019)
	IR+MW*	4	3B42 RT v7.0 uncalibrated	2000–2017	50° N-S	Huffman et al. (2007)
	IR+MW*	5	GSMaP-RNL - no gauge v6.0	2001–2013	50° N-S	Kubota et al. (2007)
	IR+MW*	6	GSMaP-NRT - no gauge v6.0	2001–2017	50° N-S	Kubota et al. (2007)
	IR+MW*	7	CMORPH v1.0 RAW	1998–2017	60° N-S	Xie et al. (2017)
	MW*	8	3B42 v7.0 MW	1998–2018	50° N-S	Huffman et al. (2007)
	IR	9	3B42 v7.0 IR	1998–2018	50° N-S	Huffman et al. (2007)
	IR	10	CHIRP v2.0	1981–2016	50° N-S	Funk et al. (2015)
Gauge-calibrated satellite (13)	IR+MW*	11	IMERG v6.0 - Final Cal	2000-2018	60° N-S	Huffman et al. (2019)
	IR+MW*	12	3B42 v7.0	1998–2018	50° N-S	Huffman et al. (2007)
	IR+MW*	13	3B42 RT v7.0	2000–2017	50° N-S	Huffman et al. (2007)
	IR+MW*	14	GSMaP-RNL - gauge v6.0	2001 -2013	50° N-S	Kubota et al. (2007)
	IR+MW*	15	GSMaP-NRT - gauge v6.0	2001–2017	50° N-S	Kubota et al. (2007)
	IR+MW*	16	CMORPH V1.0 CRT	1998–2017	60° N-S	Xie et al. (2017)
	IR+MW#	17	GPCP 1DD CDR v1.3 (yes_enforced)	1997–2017	90° N-S	Huffman et al. (2001)
	IR+MW#	18	GPCP 1DD CDR v1.3 (not_enforced)	1997–2017	90° N-S	Huffman et al. (2001)
	IR	19	PERSIANN CDR v1 r1	1983–2017	50° N-S	Ashouri et al. (2015)
	IR	20	CHIRPS v2.0	1981–2016	50° N-S	Funk et al. (2015)
	IR	21	TAMSAT v2.0	1983–2017	Africa (Land only)	Maidment et al. (2017)
	IR	22	TAMSAT v3.0	1983–2017	Africa (Land only)	Maidment et al. (2017)
	IR	23	ARC v2	1983–2017	Africa (Land only)	Novella and Thiaw (2013)

**Table 2.**

Data Type	Period	Resolution	Source
Digital Elevation Model (DEM)	2008	90 m	Consortium for spatial information ( <a href="https://cgiarcsi.community/data/srtm-90m-digital-elevation-database">https://cgiarcsi.community/data/srtm-90m-digital-elevation-database</a> )
Soil	2012	1 km	Harmonized World Soil Database v 1.1 ( <a href="http://webarchive.iiasa.ac.at/Research/LUC/External-World-soil-database/HTML/index.html?sb=1">http://webarchive.iiasa.ac.at/Research/LUC/External-World-soil-database/HTML/index.html?sb=1</a> )
Land use	2000	1 km	Global Land Cover 2000 database ( <a href="http://forobs.jrc.ec.europa.eu/products/glc2000/product.s.php">http://forobs.jrc.ec.europa.eu/products/glc2000/product.s.php</a> )
Meteorological data [daily temperature (min., max.), solar radiation, relative air humidity, wind speed]	1998 – 2012	~38 km	Climate Forecast System Reanalysis (CFSR) Model ( <a href="http://rda.ucar.edu/pub/cfsr.html">http://rda.ucar.edu/pub/cfsr.html</a> & <a href="http://globalweather.tamu.edu/">http://globalweather.tamu.edu/</a> ) Dile and Srinivasan (2014)
Precipitation data [3B42 v7.0]	1998 - 2015	0.25°	Huffman et al. (2007)
River discharge	2000 – 2012	Daily	SO-HYBAM ( <a href="http://www.so-hybam.org/">http://www.so-hybam.org/</a> ); BRLi (2016)

1060

1061

1062

1063

1064

1065

1066

1067

1068

1069

1070

1071

1072

**Table 3.**

1073

	Calibration				Validation			
	NSE	R <sup>2</sup>	PBIAS	KGE	NSE	R <sup>2</sup>	PBIAS	KGE
<b>Brazzaville/Kinshasa (outlet)</b>	0.16	0.59	14.52	0.71	0.44	0.54	4.10	0.71
<b>Kasai/Kutu-Moke</b>	0.63	0.76	-2.11	0.48	0.59	0.78	-4.66	0.48
<b>Lualaba/Kisangani</b>	0.02	0.49	7.84	0.23	0.08	0.39	-8.19	0.23
<b>Sangha/Ouessou</b>	0.67	0.71	8.37	0.80	0.59	0.65	-1.30	0.80
<b>Ubangi/Bangui</b>	0.81	0.83	4.01	0.90	0.66	0.67	-0.86	0.90

1074

1075

1076

1077

1078

1079

1080

1081

1082

1083

1084

1085

1086

1087

1088

1089

1090

1091

1092

1093



**Table 4.**

Satellite-based precipitation products	Period	Study area	Latitude	Recalibration of parameters	Highlight	Reference
3B42_v7.0 and CHIRPS_v2.0	1998 - 2010	Adige Basin (Italy)	45°N	yes	Four precipitation datasets were tested, where two were satellite-based. The satellite dataset was compared to data from de precipitation gauge stations. The results indicate the applied precipitation input influenced the estimated model parameters.	Tuo et al., 2016
IMERG_v6.0_EU, IMERG_v6.0_LU and IMERG_v6.0_FC	2014 - 2016	Kelantan Basin (Malaysia)	6°N - 4°N	yes	The satellite dataset was compared to data from de precipitation gauge stations. IMERG_FC outperformed the near real-time products in cumulative streamflow measurement. The results indicate the IMERG products could be an alternative precipitation source for this region.	Tan et al., 2018
3B42_v7.0 and IMERG_v6.0_FC	2000 - 2018	Tocantins-Araguaia basin (Brazil)	14°S - 16°S	yes	Two satellite-based precipitation products were tested. The satellite dataset was compared to data from de precipitation gauge stations. The results demonstrating the satellite dataset were able to simulate the hydrological regime adequately.	Amorim et al., 2020
3B42_v7.0 and CHIRPS_v2.0	2001 - 2012	Gurupura basin (India)	13°N - 12°N	yes	Tree precipitation datasets were tested, where two were satellite-based. CHIRPS has been tested with two different resolutions: 0.05 and 0.25. 3B42_v7.0 performed better than CHIRPS-0.05, and CHIRPS-0.25, but 3B42_v7.0 underestimated the flow for agricultural water availability in 30%.	Sharannya et al., 2020
PERSIANN-CDR_v1_r1, CHIRPS_v2.0, CMORPH_IFLOODS_v1.0, IMERG_v6.0_FC, GSMaP_gauges_v6. and 3B42_v7.0	1998 - 2019	Tarim Basin (China)	41°N	no	Seven satellite-based precipitation products were tested. The satellite dataset was compared to data from de precipitation gauge stations. The IMERG_v6.0_FC and PERSIANN-CDR_v1_r1 were the best datasets for the daily and monthly scale precipitation accuracy evaluations. PERSIANN-CDR_v1_r1 and CMORPH_IFLOODS_v1.0 performed better than others in monthly runoff simulations. All datasets have the potential to provide valuable input data in hydrological modeling.	Peng et al., 2021

CHIRPS_v2.0, 3B42_v7.0, CMORPH_CRT and PERSIANN-CDR_v1_r1	1998 - 2014	Ganjiang Basin (China)	28°N - 24°N	no	Four satellite-based precipitation products were tested. The satellite dataset was compared to data from de precipitation gauge stations. The results indicate 3B42_v7.0 provides the most accurate hydrological model simulation results, while simulated streamflow forced by CMORPH_CRT exhibits considerable underestimation of streamflow.	Wang et al., 2021
--	----------------	------------------------------	----------------	----	---	----------------------

